J. Phys. G: Nucl. Phys. 7 (1981) 687–695. Printed in Great Britain

Direct electron-pair production by muons in the energy-transfer range 3 MeV–10 GeV

M R Ghoshdastidar, G C Goswami, B Ghosh, A Paul, N L Karmakar† and N Choudhuri

Department of Physics, University of North Bengal, Darjeeling, India

Received 15 July 1980, in final form 29 September 1980

Abstract. New results from relatively high-precision measurements together with those from other more recent measurements concerning direct electron-pair production by cosmic-ray muons over a fractional energy-transfer range 1.1×10^{-3}–4.1×10^{-1} are evaluated critically in terms of more refined calculations of the direct pair production interactions with atomic nuclei and orbital electrons. This presentation reveals a greater consistency between many of the measurements and indicates the degree to which the latest theoretical predictions for the process of direct pair production agree with experiment.

1. Introduction

The direct production of electron pairs (DPP) by muons has been studied in the past and the results have been examined in some recent compilations (e.g. Grupen 1976). Many of the experiments have not been compared with the latest theoretical predictions and in some of the experiments the approximate DPP cross section formulae have been used. In the region of low energy transfer considerable deviations from the predictions have been reported in some experiments. This situation indicates the need for further investigation.

In recent years there have been new investigations of the DPP process using a 200 GeV proton beam (Butt and King 1973, Jain *et al* 1974) and a 15 GeV muon beam (Jain *et al* 1974) from accelerators. The results of the 200 GeV proton beam experimens in nuclear emulsion in the region of energy transfer less than about 0.1 GeV were found to be smaller by a factor of five than the theoretical results of Bhabha (1935). The latest experiment (Grigorov *et al* 1975), using multiply-charged cosmic-ray nuclei in the energy range 20–200 GeV/nucleon, has given results in the energy-transfer region 0.01–1 GeV which are greater by a factor of about six than the experimental cross section with a 200 GeV proton beam. Such a discrepancy has shown the urgent need for further studies of the DPP process.

On the theoretical side there are several early calculations of DPP cross sections. These calculations suffer from certain limitations. The great refinement in the calculation of Kel'ner (1967) and its extension by Kokoulin and Petrukhin (1971) has removed these limitations. Wright (1975) has provided the only experimental verification of these refined

† On leave at the University of Kiel, Kiel, West Germany.

0305-4616/81/050687 + 09 $01.50

calculations, and this is only for data in the energy-transfer range 0.1–30 GeV for a lead target.

The aim of the present investigation was to extend the experimental observation of the DPP process by muons down to an energy-transfer range of a few MeV to test the validity of various theoretical cross sections for drawing general conclusions.

2. Measurements

The present series of experiments was carried out in a large-volume multi-plate cloud chamber at sea level and underground to obtain a visual record of each event. A detailed description of the apparatus has been given in previous papers (Chaudhuri and Sinha 1964, Paul *et al* 1975a, b). Only a schematic diagram is shown in figure 1. Using thin (about 1–2 mm) targets inside the multi-plate expansion chamber in one set of observations it was possible to identify various kinds of interactions from individual events photographed by a stereoscopic camera. In another set of observations taken underground ($\sim$150 hg cm^{-2}) in the vertical direction no attempt was made to separate direct electron pairs from knock-on and bremsstrahlung interactions. At sea level observations were made in an expansion chamber operating as a muon detector of threshold energy 1 GeV at three zenith angular orientations: $\theta = 0°$, 45° and 75°. An event corresponding to the passage of a single incident muon through the apparatus was selected using a conventional multifold

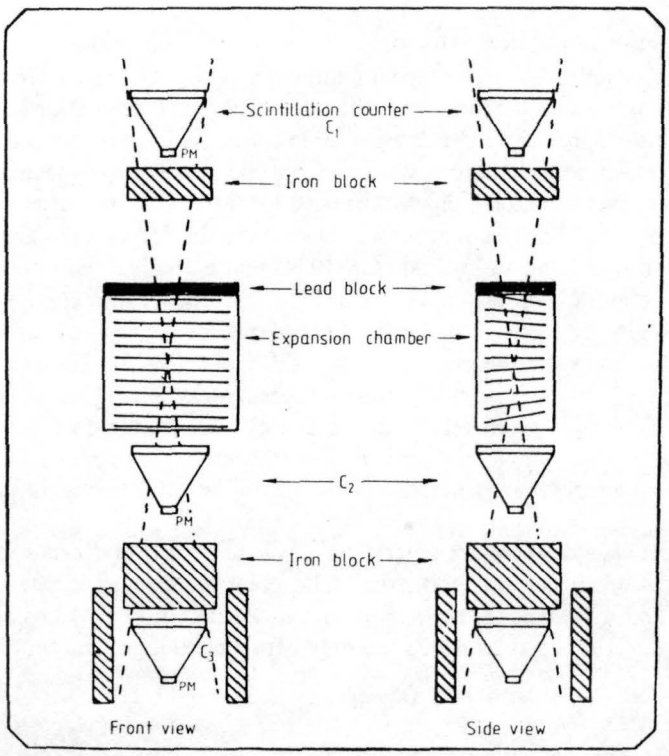

Figure 1. A schematic diagram of the experimental arrangement for visual detection of DPP events.

coincidence selection system. Photographs with tracks of singly incident primaries were examined for various kinds of interaction events.

2.1. *Theoretical: secondary energy estimation and interaction cross sections*

To analyse the experimental data, the necessary basic theoretical data include the following.

(1) The data for determining the initial energy of an electromagnetic interaction event from (*a*) the range–energy relation, (*b*) the total track length from observations at a number of observing levels in the cloud chamber and (*c*) the number of particles at the maximum of the shower event when the shower is not complete within the lowest observing level of the chamber.

(2) Theoretical electromagnetic cross sections for the various interaction processes as a function of energy transfer and primary energy.

2.1.1. Secondary energy estimate. The energy transfer, in the case of low-energy thin-target knock-on events and thin-target DPP events, was estimated using the energy-loss–range data for electrons and positrons of Berger and Seltzer (1967). Cascade multiplication and absorption effects in the targets were taken into account in the analysis of the data. Thin-target bremsstrahlung could also appear as a DPP event, but the correction for this effect was found to be negligible for the energy-transfer range of the experiment.

For high-energy events multiplying in the target itself and appearing as showers not complete within the chamber, the energy transfer was estimated from a curve like those shown in figure 2, which gives a comparison of available analytical formulations connecting shower maximum with shower energy. For showers complete within the observing levels in the chamber, for which the total electron track length could be determined, the energy transfer was also determined from the observed track length (e.g., curves C and D in figure 2). It is seen from figure 2 that shower energy estimations according to analytical formulations (Rossi 1952, Buja 1963, Thielheim and Zollner 1972) are mutually consistent.

2.1.2. Theoretical interaction cross sections. The theoretical interaction cross section for the incident spectrum of muons traversing the assembly of target plates was computed as a function of energy transfer (ε) > 3 MeV. The results for the DPP process according to the most refined calculation (based on the work of Kel'ner (1967)) of Kokoulin and Petrukhin (1971, hereafter referred to as KP) together with the Bhabha (1935) theory and the theory of Murota *et al* (1956, hereafter referred to as MUT) are shown in figure 3 for three muon energies (E). The contribution of atomic electrons to the DPP process has been taken into account through the use of the calculation of Kel'ner and Kotov (1968), which shows that the contribution of atomic electrons in the case of low-Z atoms is appreciable. For the analysis of our thick-target interaction events the theoretical knock-on cross section of Bhabha (1938) and the bremsstrahlung cross section of Petrukhin and Shestakov (1968) were combined with the DPP cross sections in the manner given previously (Chaudhuri and Goswami 1970) using the energy spectrum of muons most recently obtained by Allkofer *et al* (1971) and Nandi and Sinha (1972). These spectra agree with the more recent calculations of Badhwar *et al* (1977). The muon spectrum underground was derived using the computed theoretical total energy loss rate (Pal and Chaudhuri 1977) in rock and used for the calculation of theoretical cross sections.

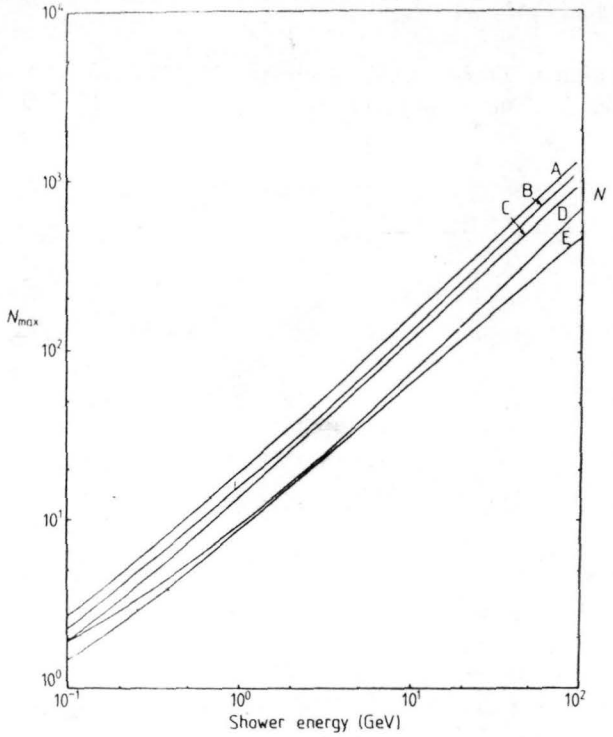

Figure 2. The relationship between the number of particles (N_{max}) at the shower maximum and shower energy for a lead target. A, from an analytical method; B, due to Theilheim and Zollner (1972); C, according to Buja (1963). Curve D is obtained according to the track length method (for a copper target) where N is the number of all track segments and curve E is obtained from an analytical method for a copper target.

3. Analysis of the experimental data and results

As mentioned in § 2, two sets of data were obtained, one with thin targets for muons incident in the vertical and inclined directions at sea level and the second set with thicker targets for muons in the vertical direction underground ($\sim$150 hg cm^{-2}). The first set includes 107 DPP events, many knock-on events and multiple electron events obtained for a total of 57 399 traversals through the multi-plate assembly containing eleven target plates. The second set of data includes 144 showers in the iron target (12.69 g cm^{-2}) and 233 showers in the lead target (70.9 g cm^{-2}) for 35 496 and 15 710 muon traversals respectively. These two sets of data were analysed separately using the information given in previous sections. The results are shown in table 1 and figure 4. The total errors indicated in table 1 and figure 4 include the statistical standard deviation on the observed number of interactions and the uncertainty arising from the estimated energy-transfer interval. The errors indicated in figures 5, 6 and 7 also include the difference between the KP prediction and that of MUT theory which has been used in many previous experiments.

4. Errors and corrections

The corrections which have been applied to the data in the manner discussed in previous

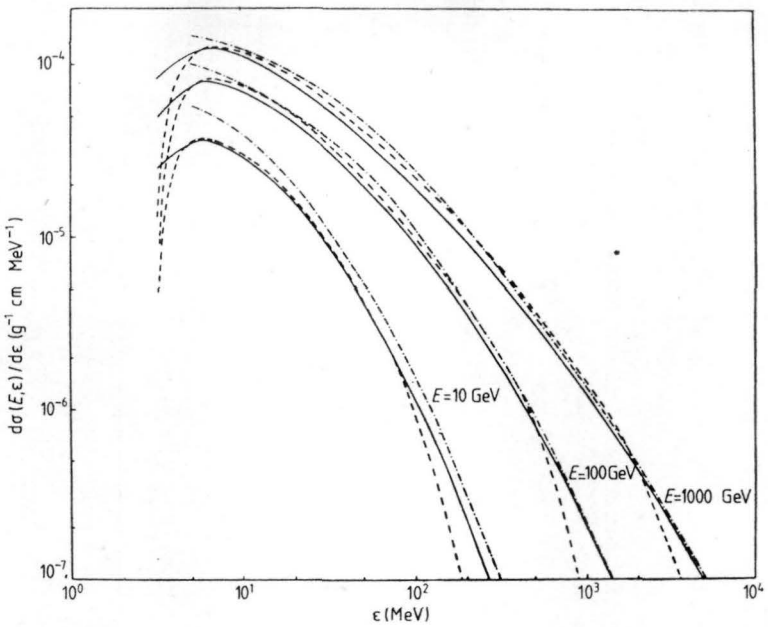

Figure 3. A plot of the differential cross section as a function of energy transfer according to the formulation of Kokoulin and Petrukhin (full curves), MUT (α, an adjustable parameter introduced to simplify angular integration at small angles, $=2$) (chain curves) and Bhabha (broken curves) for a lead target.

papers (Chaudhuri and Sinha 1964, 1965, Das and Sinha 1967, Paul *et al* 1975a, b) include the following.

(1) Pseudo-DPP production from muon bremsstrahlung.
(2) DPP electron absorption in the target.
(3) Cascade multiplication in the target of the muon knock-on electron.
(4) Double knock-on electron production in the target.

The possible systematic errors arising from (*a*) a bias in the selection of interaction events in the scanning procedure for identifying the various events for their classification, (*b*) the

Table 1. Cross section for production of direct electron pairs by muons in targets of aluminium (0.02 RU†), lead (0.29 RU) and copper (0.11 RU), for the energy-transfer range 3–50 MeV.

Mean muon energy (GeV)	Mean zenith angle (deg)	Target material	Experimental cross section (10^{-5} cm^2 g^{-1})	Theoretical cross section (10^{-5} cm^2 g^{-1})		
				KP	MUT ($\alpha=2$‡)	Bhabha
2.6	0	aluminium	(6.62 ± 2.1)	5.72	8.16	5.47
4.8	45	aluminium	(7.22 ± 2.5)	7.71	10.2	7.56
		lead	(66 ± 8)	63.5	80.3	61.8
14.4	75	copper	(29 ± 8)	27.0	33.3	26.9
		aluminium	(15 ± 4)	14.5	17.1	13.5

† RU = radiation unit.
‡ α is an adjustable parameter introduced in the MUT theory to simplify angular integration at small angles.

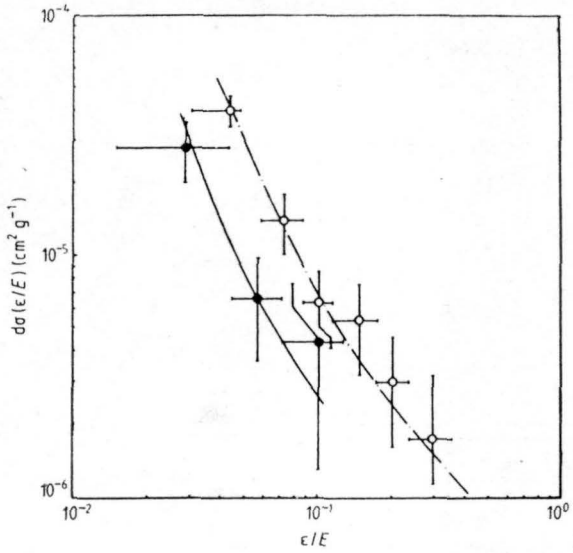

Figure 4. A plot of the differential cross sections for known-on, DPP and bremsstrahlung events in thick targets (iron: 12.6 g cm^{-2}; lead: 70.9 g cm^{-2}) as a function of (ε/E). Iron target: ——, theoretical (with KP cross section for DPP); ●, experimental. Lead target: — · —, theoretical (with KP cross section for DPP); ○, experimental. Mean muon energy = 34 GeV.

uncertainty in the event energy estimation from a count of track segments and (*c*) the uncertainty in the muon spectrum adopted for the purpose of calculating the expected

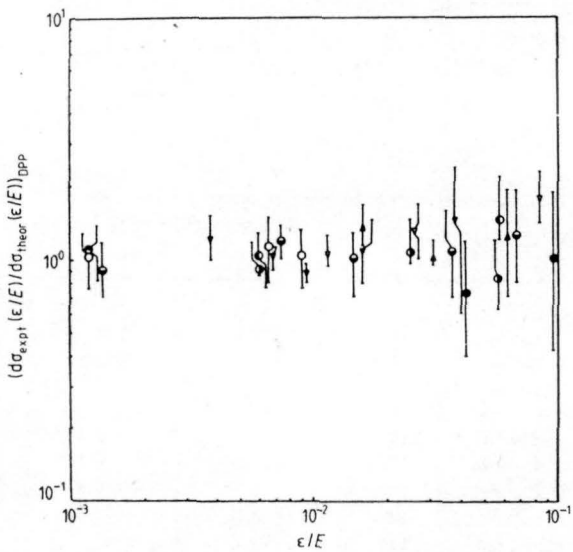

Figure 5. Plots of the measured to KP cross section for the DPP process in various target elements. ◐ (Al), ◑ (Cu) and ● (Pb): Das and Sinha (1967); mean muon energy = 6 GeV. ▼ (Fe): Stoker *et al* (1962); mean muon energy = 8.8 GeV. ▲ (Fe): Stoker *et al* (1963); mean muon energy = 3.2 GeV. ◒ (Pb): Kearney and Hazen (1965); mean muon energy = 136 GeV. ▽ (Fe): Binns and Kearney (1972); mean muon energy = 52 GeV. ◓ (Al) and ○ (Cu): present work; mean muon energy = 14.4 GeV.

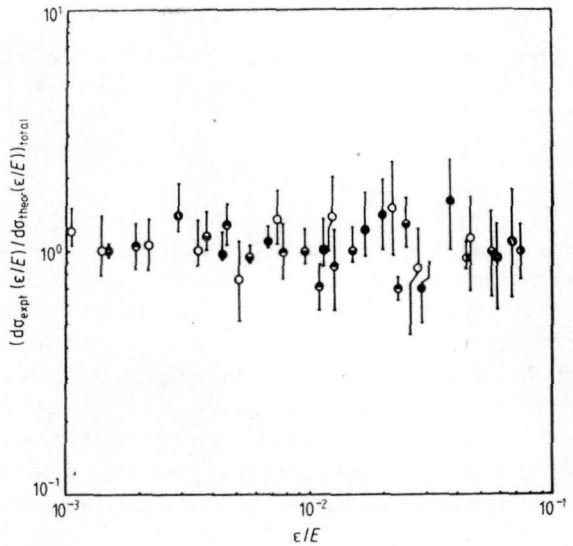

Figure 6. As figure 5, but for the sum of knock-on, DPP and bremsstrahlung cross sections. ● (Fe) and ◒ (Pb): Binns and Kearney (1972); mean muon energy = 52 GeV. ◔ (Fe): Allkofer *et al* (1971); mean muon energy = 102 GeV. ◓ (Fe): Chaudhuri and Sinha (1964); mean muon energy = 32 GeV. ○ (Pb): Kearney and Halzen (1965); mean muon energy = 136 GeV. ◘ (Fe) and ◑ (Pb): present work; mean muon energy = 34 GeV.

interaction cross section (discussed in § 2.1.2) have been reduced to a minimum by a careful experimental set-up and triggering technique, operating the multi-plate chamber under similar conditions over long periods of observation, and finally imposing a rigorous

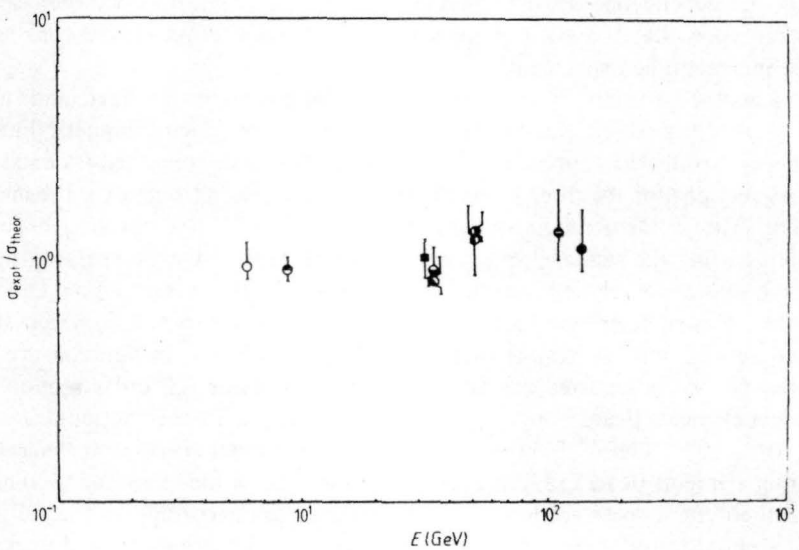

Figure 7. Plot of the data from figures 5 and 6 after integration over the energy-transfer range as a function of mean muon energy. Lead target: ◑, Binns and Kearney (1972); ●, Kearney and Hazen (1965); ◔, present work. Iron target: ◐, Binns and Kearney (1972); ■, Chaudhuri and Sinha (1964); ◓, Allkofer *et al* (1971); ◓, Stoker *et al* (1962); ◒, present work. Copper target: ○, Das and Sinha (1967).

check against any bias in the scanning procedure. In addition, the statistical uncertainty arising from the target thickness variation has been kept to a minimum.

5. Discussion and conclusion

The point to be stressed here concerns both the theory of and experiments on muon DPP processes at small and intermediate energy transfer. As mentioned before, the MUT calculations of the DPP process and the approximate formulae (based on MUT) used in previous experiments are subject to uncertainties and many of the earlier experiments found a deficit of DPP events in the low-energy region. In the present work more refined calculations on the DPP process were available for an energy-transfer range above 3 MeV for both low- and high-Z atoms, and these provided a far better theoretical basis for comparison with observation. The present thin-target DPP experimental data (table 1) were obtained without any of the uncertainties which arose from the larger target thickness used in previous experiments.

The DPP events in our second set of observations could not be separated from other thick-target interactions and only total cross sections (sum of partial cross sections for DPP, knock-on and bremsstrahlung production) were measured. Since the theories of knock-on and bremsstrahlung processes are known to a great accuracy and have also been substantiated by experiment, we have taken these cross sections as correct and drawn conclusions on the KP theory of the DPP process through a comparison of our present results on thin targets in table 1 and on thick targets in figure 4. The experimental cross sections $d\sigma(\varepsilon/E)$ in the various intervals of (ε/E), the fractional energy transfer (the fraction of the incident mean muon energy), are plotted in figure 4 at the mid-points of the intervals to show the dependence on the fractional energy transfer for two target elements. The curves represent the theoretical predictions (with the KP cross section for DPP) averaged over the incident muon spectrum.

In view of the availability of the refined calculations on DPP we have made a re-analysis of many of the previous cloud-chamber experiments on electromagnetic interactions of high-energy cosmic-ray muons. In this re-analysis, we have computed for each experiment the cross sections for the three kinds of interaction averaging each over the incident muon spectrum. The incident muon spectrum relevant to each underground experiment was determined using the sea-level muon measurements with magnetic spectrographs and the latest energy–range relation for the muon in rock. The mean muon energy in each experiment was re-determined and is indicated in figures 5, 6 and 7, which show the re-analysed results and the results of the present experiments. In figure 5 are plotted the measured DPP cross sections expressed as a fraction of the KP cross section for DPP for four target elements (lead, iron, copper and aluminium) in a wide fractional energy-transfer range 10^{-3}–10^{-1}. Figure 6 shows, for the same fractional energy-transfer range and for two target elements (lead and iron), the plot of the ratio of the measured total cross section to total theoretical cross section with the cross section according to the KP calculation. The differential cross sections recorded in figures 5 and 6 are integrated over the energy-transfer range and plotted in figure 7 to inspect the trend as a function of mean muon energy. In examining the plots of the cross section ratio in figures 5, 6 and 7 we note a consistency between all the measurements and see that the theory, with an inherent uncertainty of about 5% in the KP calculation for the DPP process, agrees better with experiment within a maximum deviation of about 25% over the whole fractional energy-transfer range 4.1×10^{-3}–1.1×10^{1}. The consistency between the KP theory and the

theory of Bhabha above $\varepsilon = 5$ MeV (figure 3) is supported by the present measurements. Thus the present work, together with the work of Wright (1975), confirms the DPP calculation of Kokoulin and Petrukhin (1971) as correct in the whole fractional energy transfer covered by these two experiments and dispels the doubt raised by the experiments of Butt and King (1973) and Jain *et al* (1974) on the validity of the theory of the DPP process.

From the present work, we may draw the following conclusion. The latest theory of the DPP process in the Coulomb field of atomic nuclei and of atomic electrons yields predictions which are in better agreement with the experimental results over a wide fractional energy-transfer range in both high- and low-Z atoms.

Acknowledgments

The authors acknowledge the provision of facilities including University Grant Commission (Government of India) Teacher Fellowships to M R Ghoshdastidar and G C Goswami, and a Research Fellowship to B Ghosh from the University of North Bengal, India.

References

Allkofer O C, Grupen C and Stamm W 1971 *Phys. Rev.* D **4** 638
Binns W R and Kearney P D 1972 *Nucl. Phys.* B **43** 402
Buja Z 1963 *Acta Phys. Polon.* **34** 381
Butt J E and King D T 1973 *Phys. Rev. Lett.* **31** 904
Berger M J and Seltzer S M 1967 *Nucl. Sci. Ser., September 15, Report 39*
Bhabha H J 1935 *Proc. R. Soc.* A **152** 559
—— 1938 *Proc. Camb. Phil. Soc.* **31** 394
Badhwar G D, Stephen S A and Golden R L 1977 *Phys. Rev.* D **15** 820
Chaudhuri N and Goswami B 1970 *Nuovo Cimento* A **65** 727
Chaudhuri N and Sinha M S 1964 *Nuovo Cimento* **32** 853
—— 1965 *Nuovo Cimento* **35** 13
Das A K and Sinha M S 1967 *Proc. Phys. Soc.* **92** 110
Grupen C 1976 *Fortschr. Phys.* **23** 127
Grigorov N L, Kondratyeva M A, Poperekova L M and Bhestopesov B Ya 1975 *Proc. 14th Int. Conf. on Cosmic Rays, Munich* **7** 2232
Jain P L, Kazuno M and Girard B 1974 *Phys. Rev. Lett.* **32** 1460
Kearney P D and Hazen W E 1965 *Phys. Rev.* **138** 173
Kel'ner S R 1967 *Sov. J. Nucl. Phys.* **5** 778
Kel'ner S R and Kotov Yu D 1968 *Sov. J. Nucl. Phys.* **7** 237
Kokuolin R P and Petrukhin A A 1971 *Proc. 12th Int. Conf. on Cosmic Rays, Hobart* **6** 2436
Murota T, Ueda A and Tanaka H 1956 *Prog. Theor. Phys.* **16** 482
Nandi B C and Sinha M S 1972 *J. Phys. A: Gen. Phys.* **5** 1384
Pal C R and Chaudhuri N 1977 *Nuovo Cimento* **37** 35
Paul A, Karmakar N L and Chaudhuri N 1975a *Proc. 14th Int. Conf. on Cosmic Rays, Munich* 1865
—— 1975b *Proc. 14th Int. Conf. on Cosmic Rays, Munich* 1983
Petrukhin A A and Shestakov V V 1968 *Can. J. Phys.* **46** S377
Rossi B 1952 *High Energy Particles* (New York: Prentice Hall)
Stoker P H, Bornman C H and Van der Merwe J P 1962 *J. Phys. Soc. Japan* **17** Suppl. A III 348
—— 1963 *Nucl. Phys.* B **45** 505
Thielheim K and Zollner R 1972 *J. Phys. A: Gen. Phys.* **5** 1054
Wright A G 1975 *J. Phys. G: Nucl. Phys.* **1** 362

IL NUOVO CIMENTO · VOL. 1 C, N. 5 Settembre-Ottobre 1978

Primary Cosmic-Ray Nucleon Spectrum from the Atmospheric Gamma-Ray and Muon Data.

M. R. GHOSHDASTIDAR, B. GHOSH and N. CHOUDHURI

Department of Physics, North Bengal University - Darjeeling, India

(ricevuto il 24 Luglio 1978)

Summary. — The available experimental inclusive cross-sections for single-pion and kaon production in proton-proton collisions between 0.01 and 2 TeV incident-proton laboratory energy have been used to determine a phenomenological form for the inclusive cross-sections. This has been used together with the recent high-precision measurements of atmospheric gamma-ray and single-muon spectra between 0.002 to 50 TeV to derive the primary nucleon spectrum in the form $I(E) = I_0 E^{-\gamma}$ up to the primary energy $\geqslant 100$ TeV. The parameters I_0 and γ vary in the range $1.75 \div 2.7$ and $2.63 \div 2.78$, respectively.

1. – Introduction.

The interrelation of the characteristics of primary cosmic-ray particles, their interactions with atmospheric matter and the secondary components has been an interesting subject of study for a long time (*e.g.* [1]). Several theoretical analyses (*e.g.* [2-6]) have been made recently on the subject. We do not discuss here the details of these treatments, but only mention that disagreement on

---

(1) G. BROOKE, P. J. HAYMAN, Y. KAMIYA and A. W. WOLFENDALE: *Proc. Phys. Soc.*, **83**, 853 (1964).
(2) I. HOFFMAN: *Phys. Rev. D*, **15**, 81 (1975).
(3) M. G. THOMSON and M. R. WHALLEY: *J. Phys. G*, **3**, 97 (1977).
(4) A. BADHWAR, S. STEPHENS and R. L. GOLDEN: *Phys. Rev. D*, **15**, 820 (1977).
(5) A. D. ERLYKIN, L. K. NG and A. W. WOLFENDALE: *J. Phys. A*, **7**, 2059 (1974).
(6) L. V. VOLKOVA and G. T. ZATSEPIN: *XV International Conference on Cosmic-Ray Physics, Bulgaria*, Vol. **6**, MN-1 (1977).

several points exists between conclusions of some of these studies. One particular point on which there is need for further analysis and the present work is done is the study of the primary cosmic-ray spectrum using the observed characteristics of secondary components: gamma-ray spectra at the top of the atmosphere and muon fluxes at sea-level and underground. This analysis is based on a new formula representing all single-pion and kaon invariant cross-sections of inclusive proton-proton (p-p) interactions in the energy range (0.012÷1.5) TeV of the incident proton in the laboratory system.

2. – Method of calculation.

We have taken in this analysis the experimentally determined cross-sections (*e.g.* ([7-9])) for single-charged-pion and kaon production in the inclusive process p+p→i+anything, for incident-proton laboratory energies in the range 0.012 to 1.5 TeV and have fitted the cross-section data to the phenomenological form for the invariant cross-section

$$(1). \qquad E\frac{\mathrm{d}\sigma}{\mathrm{d}p^3} = A_1\left[1+\frac{1}{E_p}\right]^{-n}\exp\left[-\frac{1}{E_p}\right]\exp\left[-B_1 x\right]\exp\left[-C_1 p_t\right],$$

where E_p in unit of $2m_p$ (rest mass of the p-p system) is the incident-proton laboratory energy, p_t is the transverse momentum of the particle i, $x = E/E_p$ (for $x \geqslant 0.02$), where E is the laboratory energy of the particle i. The values of the parameters of the fit to the whole set of the cross-section data are given in table I.

TABLE I. – *The values of the parameters obtained by fitting it to the measured invariant cross-section data for single-pion and kaon production.*

Particle (i)	Parameters			
	n	A_1 $\left(\mathrm{mb}/((\mathrm{GeV}^2)/c^3)\right)$	B_1	C_1 $\left((\mathrm{GeV}/c)^{-1}\right)$
π^+	1.2	102.3	4.13	5.02
π^-	4.8	112	5.43	5.16
K^+	5.8	11.9	4.26	4.14
K^-	9.8	12.9	6.82	4.81

([7]) M. G. ALBROW, A. BAGCHUS, D. P. BARBER, A. BOGAERTS, B. BOSNJAKOVIC, J. R. BROOKS, A. B. CLEGG, F. C. ERNE, C. N. P. GEE, D. H. LOCKE, F. K. LOEBINGER, P. G. MURPHY, A. RUDGE and J. C. SEN: *Nucl. Phys.*, **73** B, 40 (1974), and other references quoted therein.

([8]) P. CAPILUPPI, G. GIACOMELLI, A. M. ROSSI, G. VENNINI and B. BURSIERE: *Nucl. Phys.*, **70** B, 1 (1974).

([9]) E. YEN: *Phys. Rev. D*, **10**, 836 (1974).

The function (1) gives a good fit (χ^2 per degree of freedom in the range 0.85 to 1.5 for the whole incident-proton energy range of 0.012 to 1.5 TeV). The p_t range is from 0.1 to 0.8 GeV/c over $x = 0.05$ to 0.8.

2·1. *Calculation of production spectra of cosmic-ray mesons.* – We have applied (1) to calculate the production spectrum of cosmic-ray mesons produced when protons and other nuclear components of the primary beam interact with air nuclei. The effects of target in nucleon-nucleus collision and of nucleus-nucleus collision may not be important for the present analysis and are not considered.

For the nucleon-nucleon process at a given incident energy and x value, the number distribution of the produced particles i in the collision is given by

$$x\frac{\mathrm{d}\sigma}{\mathrm{d}x} = E\frac{\mathrm{d}\sigma}{\mathrm{d}E} = \pi\int E\frac{\mathrm{d}\sigma}{\mathrm{d}p^3}\,\mathrm{d}p_t^2\,. \tag{2}$$

If the spectrum of incident nucleons is a power law $E_p^{-\gamma}\mathrm{d}E_p$, then the production spectrum of secondary mesons i of energy E is obtained from (2) as

$$F_i(E)\,\mathrm{d}E = I(E)\frac{1}{\sigma_{\mathrm{inel}}}\left[\int x^{\gamma-1}\frac{\mathrm{d}\sigma}{\mathrm{d}x}\,\mathrm{d}x\right]\mathrm{d}E = I(E)f_i\,\mathrm{d}E\,, \tag{3}$$

where σ_{inel} is the total inelastic cross-section of p-p interaction and is taken here as constant at 35 mb from recent accelerator experiments (*e.g.* [10]). The spectra of different components, except the Fe group of nuclei [11], of the primary beam are assumed to be represented by the power law with an exponent γ same as that of the primary « all nuclei » spectrum. It is further assumed that nucleons in the incident nuclei behave as if they were free nucleons when they interact with air nuclei. The spectrum of the primary total nucleon beam can thus be expressed in terms of the number of nucleons in unit interval of energy E_p per nucleon by

$$I(E_p)\,\mathrm{d}E_p = I_0 E_p^{-\gamma}\,\mathrm{d}E_p\,, \tag{4}$$

where γ is different in different energy regions. Using this incident-nucleon spectrum (4) with several chosen values of γ in different primary-energy regions, the production spectra of cosmic-ray pions and kaons have been calculated.

---

[10] E. Amaldi, R. Biancastelli, C. Basic, G. Matthias, J. V. Allaby, W. Bartel, G. Cocconi, A. N. Diddens, R. W. Dobinson and A. M. Wetherell: *Phys. Lett.*, **44** B, 112 (1973).

[11] Y. K. Balsurhamanyan and J. F. Ormes: *Ast. Phys.*, **186**, 109 (1973).

3. – Derivation of the primary nucleon spectrum.

3·1. *Relationship between primary spectrum and gamma-ray spectrum at the top of the atmosphere.* – The main source of gamma-rays at the top of the atmosphere is the decay of neutral pions which are produced along with charged pions in collisions of primary cosmic-ray nucleons with air nuclei. As the neutral pions decay instantaneously into two gamma-photons, the production spectrum of gamma-rays at energy E' is

$$F(E')\,\mathrm{d}E' = \mathrm{d}E' \int_{E=\varepsilon}^{\infty} \frac{1}{2}\,[F(E_{\pi^+}) + F(E_{\pi^-})]\,\frac{2\,\mathrm{d}E}{\psi(E)}\,,$$

where

$$\psi(E) = [E^2 - m_{\pi^0}^2]^{\frac{1}{2}} \quad \text{and} \quad \varepsilon = E' + \frac{m_{\pi^0}^2}{4E'} \approx E' \quad \text{for large } E'\,.$$

The gamma-ray spectrum at depth X g cm^{-2} from the top of the atmosphere is

$$\gamma(E')\,\mathrm{d}E'\,\mathrm{d}X = I(E')\,\frac{f_{\pi^+} + f_{\pi^-}}{\gamma}\,\exp\left[-\frac{X}{\lambda_a}\right]\frac{\mathrm{d}X}{\lambda}\,, \tag{5}$$

where $I(E')$ is the primary cosmic-ray nucleon spectrum at energy E' and $f_{\pi^\pm}$ is defined in (3); λ and λ_a, the interaction and attenuation mean free paths in air of nucleons generating pions, are taken to be constant with values 80 g cm^{-2} and 120 g cm^{-2}, respectively.

3·2. *Relationship between primary spectrum and sea-level muon spectrum.* – We first make a simplified calculation to correlate the incident-primary-nucleon spectrum and sea-level muon spectrum in the vertical direction. We consider in this approach only generation of muons from decay of first generation of mesons i (pions and kaons).

The spectra of mesons from pion-muon and kaon-muon decay (branching ratio $\frac{2}{3}$) at any vertical depth X are given by the solution of the diffusion equation (by neglecting the energy loss term)

$$\frac{\partial \mathcal{N}_i(E, X)}{\partial X} = -\mathcal{N}_i(E, X)\left[\frac{1}{\lambda_i} + \frac{h}{X}\right] + \frac{F_i(E)}{\lambda}\exp\left[-\frac{X}{\lambda_a}\right], \tag{6}$$

where $\mathcal{N}_i(E, X)$ is the spectrum of mesons i at energy E, $F_i(E)$ is the production spectrum given by (3) and λ_i ($\lambda_\pi = 120$ g cm^{-2} and $\lambda_K = 150$ g cm^{-2}) is the interaction mean free path of mesons i, $h_i = Hm_i c/\tau_i E_i = b_i/E_i$,

H is the scale height ($6.4 \cdot 10^5$ cm at $X = 100$ g cm^{-2}). The solution of the diffusion equation (6) is used to obtain the sea-level muon spectrum due to the decay of mesons i in the form

$$\mathcal{N}_\mu(E_\mu, X)\,\mathrm{d}E_\mu = \mathrm{d}E_\mu \int_{E_\mu}^{(m_i/m_\mu)^2 E_\mu} \int_X \frac{1}{\lambda} \frac{m_i^2}{m_i^2 - m_\mu^2} \exp\left[-\frac{X}{\lambda_a}\right] \mathrm{d}X\, F_i(E) \Lambda(\mathcal{G}, h) \frac{\mathrm{d}E_i}{E_i},$$

where

$$\mathcal{G} = \frac{X}{L'} \quad \text{and} \quad \frac{1}{L'} = \frac{1}{\lambda} - \frac{1}{\lambda_a},$$

$$\Lambda(\mathcal{G}, h) = h_i \int_0^1 t^h \exp[\mathcal{G}(1-t)]\,\mathrm{d}t,$$

$$t = 1 \quad \text{at} \quad X_0 = 1030 \text{ g cm}^{-2} \text{ (sea-level)}.$$

The integration over X and then over E_i gives at sea-level

$$\mathcal{N}_\mu(E_\mu, X)\,\mathrm{d}E_\mu = \frac{1}{\alpha + \gamma} \left[\frac{1 - (m_\mu/m_i)^{2(\alpha+\gamma)}}{1 - (m_\mu/m_i)^2}\right] M(h_\mu) F(E_\mu)\,\mathrm{d}E_\mu, \tag{7}$$

where

$$M(h_\mu \gg 1) \simeq \frac{h_\mu}{h_\mu + 1} \frac{\lambda_a}{\lambda},$$

$$M(h_\mu \ll 1) \simeq \frac{h_\mu \lambda_a}{\lambda_a - \lambda} \ln(\lambda_a/\lambda), \qquad h_\mu = \frac{b_\pi}{E_\mu},$$

$$F(E_\mu) = I(E_\mu) f_i$$

and

$$\alpha = \left[1 + \frac{h_i \lambda \ln(\lambda_a/\lambda)}{\lambda_a - \lambda}\right]^{-1}.$$

4. – Improved calculation of sea-level muon spectra.

The generation of mesons from secondary pion collisions with air nuclei is taken into account by folding it with the production spectrum of the secondary mesons from primary nucleon-nucleus collisions. The production spectrum of mesons i at a depth X' in the atmosphere and local zenith angle $\theta(X')$

is taken as

$$\mathcal{N}_i(E'X'\theta(X'))\mathrm{d}E'\,\mathrm{d}X' = \frac{F_i(E')}{\lambda}\sec\theta(X')\mathrm{d}X'\exp\left[-\int_0^{X'}\frac{\sec\theta(X'')}{\lambda'}\mathrm{d}X''\right]\mathrm{d}E'.$$

The differential spectrum of mesons at X is

$$\mathcal{N}_i(EX\theta(X))\mathrm{d}E = \int_0^X\left(\frac{F_i(E')}{\lambda}\sec\theta(X')\exp\left[-\int_0^{X'}\frac{\sec\theta(X'')}{\lambda'}\mathrm{d}X''\right]\right)\mathrm{d}E\cdot$$

$$\cdot\left(\exp\left[-\int_{X'}^{X}\left[\frac{1}{\lambda_i}+\frac{b_i}{E_i''\varrho(X'')}\right]\sec\theta(X'')\mathrm{d}X''\right]\right)\sec\theta(X')\mathrm{d}X',$$

where the expression in the second parentheses is the probability that mesons i produced at X' reach at depth X, $\varrho(X'')$ is the density of air at depth X'', λ' is the attenuation mean free path of all hadrons generating pions with a constant value of 120 g cm^{-2}.

At the observation level depth X_0 and zenith angle θ the differential muon spectrum is

$$\mathcal{N}_\mu(EX_0\theta) = \int_{E_\mu}^{(m_i/m_\mu)^2E_\mu}\int_X\frac{b_i\sec\theta(X)}{\varrho(X)}\frac{m_i^2}{m_i^2-m_\mu^2}\cdot \tag{8}$$

$$\cdot W(EXX_0\theta(X))\mathcal{N}_i(EX\theta(X))\frac{\mathrm{d}E_i}{E_i^2}\mathrm{d}X,$$

where $W(EXX_0\theta(X))$ is the probability that muons produced at depth X can reach with energy E at depth X_0. At near horizontal incidence, this is expressed (see [12]) in terms of local zenith angle $\theta(X)$, at depth X of the muon path. The integral flux is

$$I(>E) = \int_E^\infty \mathcal{N}_\mu(EX\theta)\mathrm{d}E. \tag{9}$$

5. – Predictions for primary cosmic rays.

To deduce information on the primary cosmic-ray spectrum, we start with (3) and (4) and the observed gamma-ray spectral data [13] to calculate $I(E)$ using (5). For this we have chosen $\gamma = 2.6$, $\gamma = 2.75$ as trial index values of the primary nucleon spectrum below 0.1 TeV and above 0.1 TeV, respectively. The connection given by (7) between primary nucleon spectrum and the sea-

---

([12]) K. MAEDA: *Fortschr. Phys.*, **21**, 113 (1973).

([13]) K. C. ANAND, R. R. DANIEL and S. A. STEPHENS: *Pramana*, **1**, 1 (1973).

level muon spectrum has been used to derive $I(E)$ by using recent measurements ([14-17]). The trial values of γ used in this derivation are

$$\gamma = 2.60 \quad \text{for} \quad E < 1 \text{ TeV},$$
$$\gamma = 2.75 \quad \text{for} \quad E > 1 \text{ TeV},$$
$$\gamma = 2.9 \quad \text{for} \quad E > 5 \text{ TeV}.$$

The derived spectral forms obtained from a least-square analysis of the calculated intensities are given in table II.

TABLE II. – *The derived primary nucleon spectrum* $I(E) = I_0 E^{-\gamma}$ (nucleons/cm^2 sr s GeV/nucleon).

Chosen value of the exponential (γ)	Energy interval (TeV)	([a])	([b])
2.6	< 1	$0.32\,E^{-2.6}$	$0.98\,E^{-2.63}$
2.75	≥ 1	$2.56\,E^{-2.78}$	$1.96\,E^{-2.74}$
	$5 \div 9$	—	$2.6\ E^{-2.78}$
2.9	$5 \div 9$	—	$3.9\ E^{-2.92}$

([a]) Derived from observed gamma-ray spectrum at the top of the atmosphere.
([b]) Derived from observed sea-level muon spectra.

In fig. 1 the calculated spectra with $\gamma = 2.75$ in the energy interval $(0.1 \div 9)$ TeV are referred to the observed total primary nucleon intensities derived from a recent compilation ([18]) which includes very recent measurements on H+He, C+O and Fe+Ni up to a few hundred GeV per nucleon, measurements by GRIGOROV *et al.* ([19]) on protons up to about 100 TeV. The figure shows that the consistency exists with direct observations in the lower-energy regions, where the nuclear composition of the primary has been determined and is well known.

([14]) C. A. AYRE, J. M. BAXENDALE, C. J. HUME, B. C. NANDI, M. G. THOMPSON and M. R. WHALLEY: *J. Phys. G*, **1**, 584 (1975).
([15]) O. C. ALLKOFER, K. CARSTENSEN and W. D. DAU: *Phys. Lett.*, **36** B, 425 (1971).
([16]) C. A. AYRE, J. M. BAXENDALE, J. DANIEL, C. J. HUME, M. G. THOMPSON, M. R. WHALLEY and A. W. WOLFENDALE: *Proceedings of the XIII International Conference on Cosmic Rays*, Vol. **3** (Denver, Colo., 1973), p. 1954.
([17]) A. N. AMENOVA: Report of Nucl. Phys. Lab. Moscow, reference in *XV International Conference on Cosmic Rays, Bulgaria*, Vol. **6**, MN-6 (1977).
([18]) E. JULIUSSON: *Proceedings of the XIV International Conference on Cosmic Rays*, Vol. **8** (Munich, 1975), p. 1679.
([19]) N. L. GRIGOROV, V. E. NESTEROV, I. D. RAPOPORT, I. A. SAVENKO and G. A. SKURIDIN: *Sov. Journ. Nucl. Phys.* (*Yad. Fiz.*), **11**, 588 (1058) (1970).

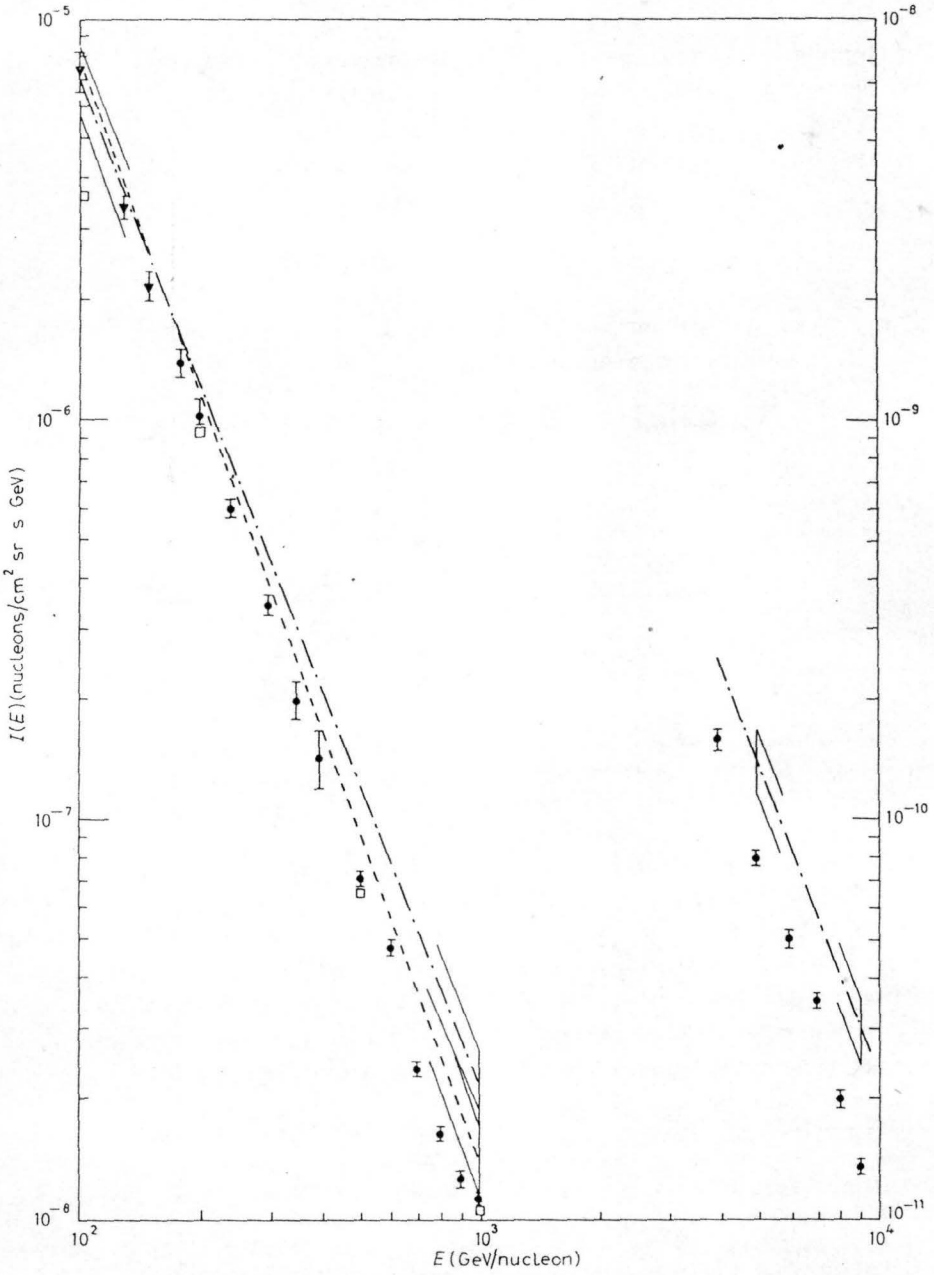

Fig. 1. – The derived primary nucleon spectra with results from recent measurements on primary components. The uncertainty limits of the calculated spectrum are indicated only at the extremes. • protons ([19]), ▾ (H+He)+(C+O)+(Fe+Ni) nucleons ([18]), ▫ (H+He) nucleons ([20]). Present work: —·—·— from muon spectrum, — — — from gamma-ray spectrum.

([20]) M. J. RYAN, V. K. BALSUBRHAMANYAN and J. F. ORMES: *Hobart Cosmic-Ray Conference Papers* 1, paper OG 54, p. 173 (1971); and also *Phys. Rev. Lett.*, **28**, 985 (1972).

5·1. *Final estimate of primary spectrum.* – The differential and integral muon intensities due to $\pi \to \mu + \nu$ and $K \to \mu + \nu$ decay modes have been computed from (8) and (9) by using the nucleon spectra in table II as trial spectra in the relevant energy regions. The computed intensities are then compared with recent high-precision sea-level and underground measurements of muon fluxes.

The measured muon intensities for the present comparison come from the following works:

1) ALLKOFER *et al.* [15], vertical differential muon spectra at sea-level, energy range $(0.0002 \div 1)$ TeV;

2) AYRE *et al.* [16], vertical differential muon spectrum at sea-level, energy range $(0.02 \div 0.5)$ TeV;

3) IIDA [21], sea-level differential muon fluxes at zenith angle $\theta = 85°$, energy range $(0.02 \div 1)$ TeV;

4) AMENOVA [17], vertical differential muon fluxes at sea-level, energy range $(5 \div 9)$ TeV;

5) KRISHNASWAMY *et al.* [22,23], MIYAKE *et al.* [24], underground integral intensity measurements, depth range $(3000 \div 9500)$ hg cm^{-2} in Kolar Gold fields (India), energy range $(1 \div 50)$ TeV.

The underground integral intensities *vs.* depth relation was converted to integral energy spectrum by using the accurately computed energy loss rate in rock [25]. The procedure followed in comparison was to use the relation $E_p = (1/\langle x \rangle)(E_\pi/E_\mu) E_\mu$ between muon energy and primary nucleon energy at the first collision in the atmosphere and then make the comparison, « observed intensity/calculated intensity » in the equivalent muon energy region approach, very close (within a maximum of ten percent) to the exact agreement point. In each energy region this was done by adjusting the trial primary-spectrum parameter I_0 to a fixed value for best overall agreement. The final spectral results thus obtained are

$$I(E) = 1.75\, E^{-2.63}, \qquad E < 5 \text{ TeV/nucleon},$$

$$I(E) = 2.2\, E^{-2.74}, \qquad 5 < E < 100 \text{ TeV/nucleon},$$

---

[21] S. IIDA: *Nuovo Cimento*, **26** B, 559 (1975).

[22] M. R. KRISHNASWAMY, M. G. K. MENON, V. S. NARASIMHAM, S. A. KAWAKAMI, S. MIYAKE and A. MIZOHATA: *Proceedings of the XI International Conference on Cosmic Rays (Budapest), Acta Phys. (Hungary)*, **29**, Suppl. 4, 221 (1969).

[23] M. R. KRISHNASWAMY, M. G. K. MENON, V. S. NARASIMHAM, K. HINOTANI, N. ITO, S. MIYAKE, J. I. OSBORNE, A. J. PARSONS and A. W. WOLFENDALE: *Proc. Roy Soc.*, **223** A, S11 (1971).

[24] S. MIYAKE, V. S. NARASIMHAM and P. V. RAMANAMURTHY: *Nuovo Cimento*, **32**, 1505 (1964).

[25] C. R. PAUL and N. CHOUDHURI: *Nuovo Cimento*, **37**, 35 (1977).

and

$$I(E) = 2.7\, E^{-2.78}, \qquad E > 100 \text{ TeV/nucleon}.$$

6. – Discussion and conclusion.

The analysis outlined above is based on the use of the single-particle inclusive distribution (4) in the energy range below 2 TeV to all higher-energy interactions, and an assumed constant value of the total inelastic cross-section of the p-p collision. The procedure adopted here leads to the exploration of the characteristics of hadronic interactions at very high energies and the determination of primary nucleon spectrum by examining the spectra of secondary gamma and muon components. The information about the primary cosmic-ray composition can also be inferred from our derived spectral forms by comparing with that obtained by working back from an assumed primary mass composition independent of primary energy per nucleon. The conclusions to be drawn from this analysis are as follows:

1) The experimental single-pion and kaon inclusive cross-sections determined at energies below 2 TeV can interpret hadronic interactions in cosmic rays up to a primary energy of a few hundred TeV.

2) The differential primary nucleon spectrum in $(0.01 \div 100)$ TeV/nucleon and above is found to be represented by a simple power law $I_0 E^{-\gamma}$ with I_0 and γ changing slowly in the range $1.75 \div 2.7$ and $2.63 \div 2.78$, respectively. This spectrum joins smoothly to that with an exponent 2.8 in the higher-energy region (above 10^3 TeV) from very recent measurements of extensive air showers.

3) The derived differential spectrum does not reflect any sudden deviation of the primary composition from the average « all nuclei » composition at the highest-energy region considered in the present analysis.

● RIASSUNTO (*)

Sono state usate le sezioni d'urto inclusive sperimentali disponibili per la produzione di pioni singoli e kaoni negli urti protone-protone ad una energia del protone incidente nel laboratorio compresa tra 0.01 e 2 TeV per determinare una forma fenomenologica per la sezione d'urto inclusiva. Questa è stata usata assieme a recenti misure ad alta precisione dei raggi gamma e degli spettri di muoni singoli tra 0.002 e 50 TeV per derivare lo spettro primario dei nucleoni nella forma $I(E) = I_0 E^{-\gamma}$ fino a un'energia primaria $\geqslant 100$ TeV. I parametri I_0 e γ variano nell'intervallo $1.75 \div 2.7$ e $2.63 \div 2.78$ rispettivamente.

(*) *Traduzione a cura della Redazione.*

Nuclear Instruments and Methods 192 (1982) 375–378
North-Holland Publishing Company

A SIMPLE ADC UNIT FOR COSMIC RAY AIR SHOWER EXPERIMENTS

A. GOSWAMI, B. GHOSH, M.R. GHOSHDASTIDAR, S.K. SENGUPTA and N. CHAUDHURI
Department of Physics, University of North Bengal, Darjeeling, India

Received 10 November 1980 and in revised form 14 April 1981

The design of a new low cost analog-to-digital converter system is described. It is based upon the method of linearising the charging process of a storage condenser and is controlled by logic gates. Its tested characteristics have been found to be reliable for application in cosmic ray air shower experiments.

1. Introduction

The digital encoding of pulse height in nuclear pulse techniques with the method of Wilkinson [1] for digital measurements has succeeded over some other methods for digitisation of analog pulses. Manfredy and Rimini [2], among others, have described a Wilkinson type analog-to-digital converter (ADC), based upon the method of linearisation of the discharging process of a storage condenser. The method of Wilkinson has been used in the present work to design a new analog-to-digital converter based upon the technique of linearising the charging process of a condenser for use in nuclear physics and cosmic ray air shower experiments. The design, operation and performance of the converter are described in this paper.

2. Principle of operation

The operation of the converter starts with the charging of a condenser by means of a constant current source (linear ramp generator) to a voltage equal to the input pulse amplitude to be measured. The charging time of the condenser to a voltage equal to the input voltage is measured by means of a 1 MHz clock pulse. The operating principle is indicated in fig. 1. As the condenser voltage rises linearly to the input voltage, the number of clock pulses counted during the capacitor charging time is therefore proportional to the input voltage. The new design for the realisation of the converter is described in the following section.

3. Description of the converter circuit

The circuit diagram of the converter is shown in fig. 2. The whole circuit consists of two parts: (1) the ADC consisting of four operational amplifiers, two silicon transistors (T_1, T_2) and two TTL ICs (IC-5, IC-6), (2) a built-in-programmer consisting of logic gates and counters indicated in fig. 2.

In the ADC circuit the transistor T_1 acts as a constant current source to charge the capacitor C connected to the collector of T_1 and T_2. The voltage follower IC-1 connected to the capacitor C is meant to give information about the voltage across C to the comparator IC-3. The transistor T_2 acts as an analog switch across the capacitor C.

The analog input pulse is fed to the comparator through a summing amplifier, the inverting input of the amplifier is connected to a preset for setting the output of the comparator at a zero logic level when the input voltage is at zero level. This occurs due to low voltage on the collector of T_2 in the conducting state. The output voltage of the comparator IC-3 is clipped at a high logic level and connected to the input of an inverting logic gate G_1. The output of the inverter is connected to the "reset to zero" (R_0) input of a decade counter, IC-6. The output of G_1 is further inverted by G_2 and then applied to one of the inputs of the trigger controlling gate G_3. This input, directly related to the voltage setting time of the analog multiplexer, will not allow any start pulse to the ADC until the voltage is set for scanning. The output of the gate G_3 is connected to the "Rest to Nine" (R_9) input of IC-6 whose outputs Q_A and Q_D are used to control the ramp generator as these two

0029-554X/82/0000–0000/$02.75

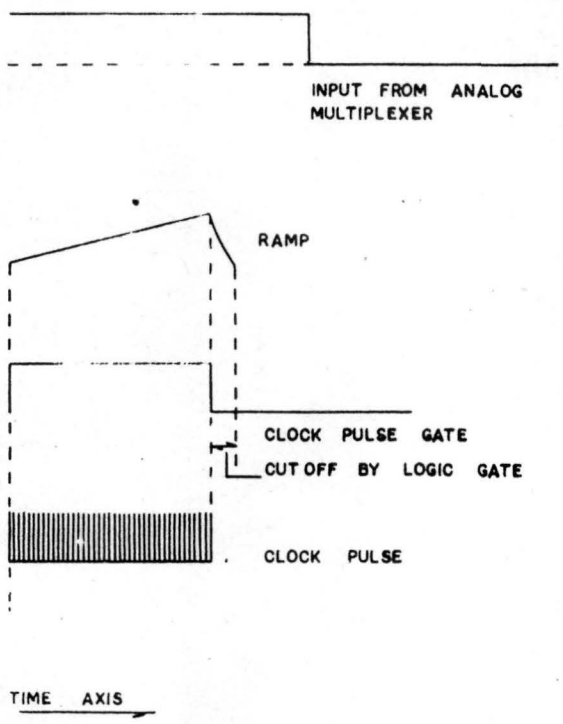

Fig. 1. Principle of the ADC.

change their logic states with R_0 and R_9. Here decade counter (IC-6) is used for "preset' and "clear" purposes. Any flip-flop with "preset" and "clear" can be used instead of IC-6. But such a flip-flop should be properly gated to that when any one of "preset" and "clear" goes low the other should remain high. But in case of decade counter no such gate is necessary. The output Q_D of the IC-6 is connected to one of the inputs of the Schmidt trigger IC-5 containing a 1 MHz clock pulse and also the inverting input of the high speed operational amplifier IC-4 of unit gain. Instead of a Schmidt trigger (IC-5) a simple AND gate can be used provided the input 1 MHz clock is a Schmidt triggered output to avoid errors that may occur in the counters which follow the ADC and which are very susceptible to noise. The output of IC-4 is connected to the base of T_2. The noninverting input of IC-4 is connected to a 10 kΩ resistor preset to apply a positive of IC-11 is used to reset the analog multiplexer. T_2 goes negative and when Q_D is low the base of T_1 goes positive just to make T_2 conducting. The output of IC-5 gives the serial data output which can be connected to counters for parallel data output.

The built-in programme is an assembly of different logic gates (G_3–G_9), counters (IC-9 to IC-12) and

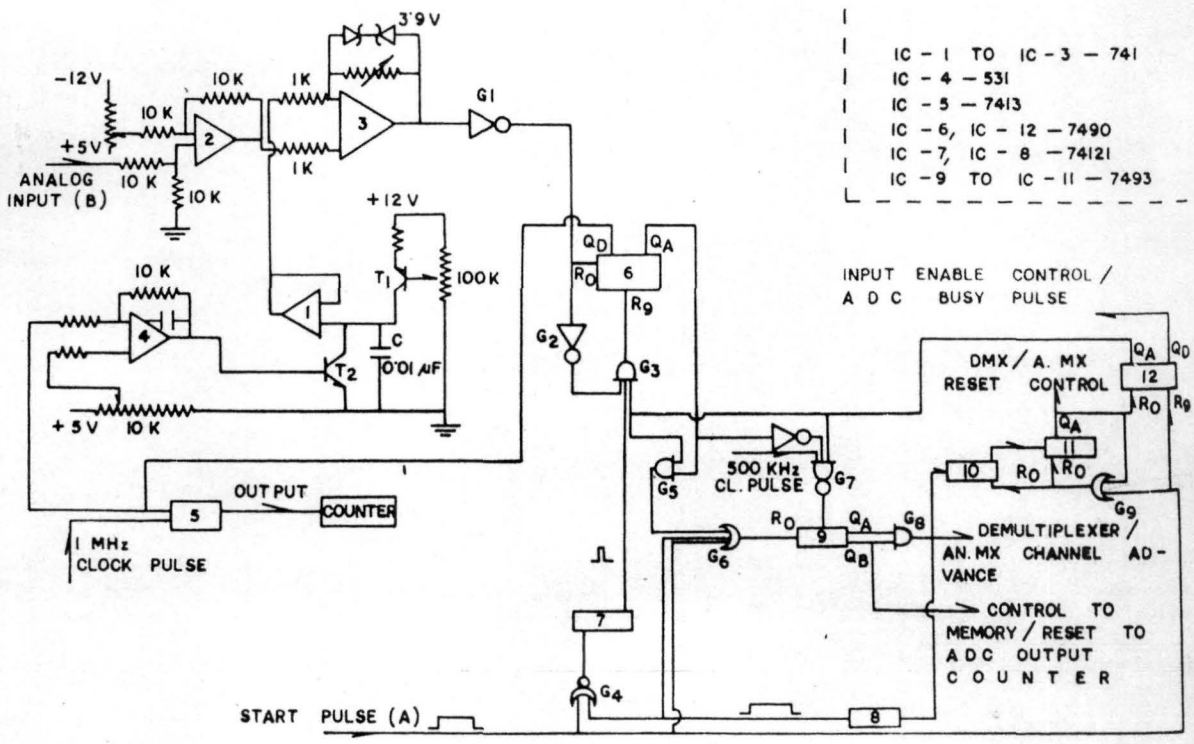

Fig. 2. Circuit diagram of the converter.

monostable multivibrators (IC-7, IC-8). The monostable multivibrator IC-7 triggers the ADC and IC-8 allows the voltage setting time of the analog multiplexer. For analysis with 16 channels, the output Q_A of IC-11 is used to reset the analog multiplexer, demultiplexer address register, the preset counters (IC-10 and IC-11) and programme controller IC-12.

4. Operation of the circuit

The unit IC-12 which controls the whole programme is normally reset to zero when the ADC will not scan any input voltage applied at the analog input terminal B. Whenever there is an input voltage, a positive start pulse derived from the control unit of the system where this ADC is intended to be used, is applied to the "start pulse" input terminal A. The width of the start pulse is slightly greater than the voltage setting time of the analog multiplexer with its output point connected to the analog input terminal B. The positive edge of the start pulse resets the IC-12 to nine (R_9) and IC-9, IC-10 and IC-11 to zero (R_0) through gates G_6 and G_9. The output Q_D of IC-12 after being inverted connects the analog multiplexer and demultiplexer to the ADC through "input enable control" and the output Q_A of IC-12 sets one of the inputs of gates G_3 and G_7 high. The input voltage makes the comparator IC-3 output high making R_0 of IC-6 low. The IC-7 is triggered at the end of the start pulse to reset IC-6 to nine (R_9) so that Q_A and Q_D of IC-6 are high. The width of the triggering pulse must be less than 1 μs for 1 MHz clock pulse. The output Q_D makes the base of T_2 negative and opens the 1 MHz clock pulse to the ADC counter and the storage capacitor starts charging at a constant current via T_1 until the output of comparator IC-3 goes to zero logic level making R_0 of IC-6 high. As R_0 of IC-6 goes high, the output Q_D of IC-6 becomes low stopping the 1 MHz clock pulse to the counters and making the base of T_2 positive to enable the capacitor C to discharge. Here the transistor T_2 is switched on and off by an operational amplifier (IC-4) but not by conventional TTL levels. This is done for the reason that logic low levels sometimes give ~0.1 V or even ~0.2 V. It is observed that there is a low conduction current through the transistor T_2 which affects the linearity between the digital output and the analog input. Replacing T_2 by a field effect transistor (FET) BFW 11 gives better result. With BFW 11 the gain of IC-4 is made about 3 so that when Q_D of IC-6 is low the gate of BFW 11 goes to about 1 V and when Q_D is high the gate goes to less than −4 V which is equal to the drain current cut-off voltage for BFW 11. At the end of the conversion the discharge of the capacitor C takes place through the FET. The FET being a better electronic switch than a silicon transistor, the discharge of the capacitor C is very fast to make the ADC ready for the next scan. The [illegible] Q_A of IC-6 being low, the output of G_5 is low [illegible] there is no start pulse either at the input B or from IC-8 the output of G_6 is also low, making R_0 of IC-9 low. The 500 kHz clock pulse now enters the counter IC-9. The outputs Q_A and Q_B of IC-9 through G_8 increase the preset counter reading and the analog multiplexer and demultiplexer channel address by unity and produce another start pulse at the monostable multivibrator IC-8. As soon as the start pulse is generated, R_0 of IC-9 goes high through G_6 and the 500 kHz clock pulse entry to IC-9 is cut off starting a new cycle of operation. At the end of the sixteenth cycle, the output Q_A of IC-11 goes high, thus resetting the preset counter and the programme controlling IC-12 to zero, making the whole system ready for a new cycle of operations.

5. Discussion

The circuit described above has been operated for a long time and is now standardised for use in cosmic ray air shower experiments. The voltage ramp of the linear ramp generator has been photgraphed in a large number of test operations. The ramp has a fairly constant slope and good linearity up to 10 V. For a charging current corresponding to 10 mV/μs, the differential non-linearity is $<\pm 1\%$ for an input voltage higher than 50 mV but less than 10 V. Non-linearity above 10 V and can be achieved by operating the transistor T_1 with a higher voltage (15 V).

As 1 MHz quartz oscillator is used in the test circuit. The clock oscillator and the ramp generator are controlled by logic gates and hence all possible errors at small input voltages are expected to be negligible. Since R_9 overrides R_0, there may be an inaccuracy at zero input voltage of one channel width if the start pulse to IC-6 synchronises with the high logic level of the clock pulse. This can be avoided by interchanging "reset to nine" (R_9) with "reset to zero" (R_0) and by inverting outputs Q_A and Q_D of IC-6.

Fig. 3 shows the relation between the digital output and the analog input. The digital output of the

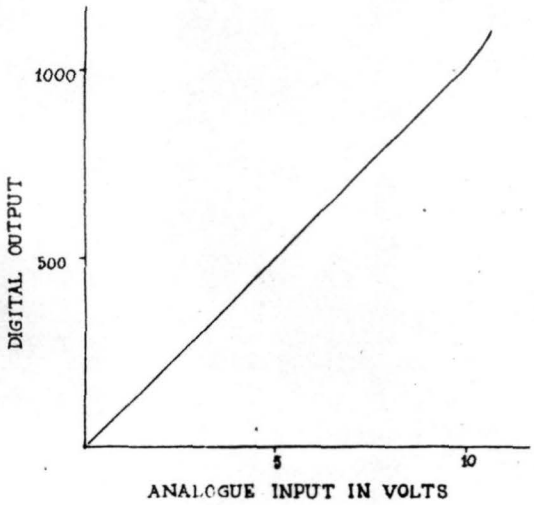

Fig. 3. Relation between the digital output and the analog input.

ADC for a particular height of an analog pulse is not constant but can be adjusted. To fix the digital output at a particular value the bias of the transistor T_1 is adjusted which controls the charging rate of the capacitor C. For a digital output 100 per volt with 1 MHz clock pulse the conversion time is 100 μs/V, But using a 10 MHz clock and adjusting the digital output 100 per volt the conversion time becomes 10 μs/V. In both cases the resolution is 10 mV. This resolution can be made 1 mV by making the digital output 1000 per volt by adjusting the charging rate of the capacitor C through transistor T_1. In this case the conversion time becomes 100 μs/V using a 10 MHz clock pulse. It may be mentioned that all operational amplifiers 741 should be replaced by 715. This is the main advantage of the ADC where we can adjust the conversion time and resolution according to need. The cost of the built-up ADC is at the level of one hundred rupees. The cost of similar such indigeneous ADCs is higher by at least a factor of four.

The authors acknowledge the provision of facilities including UGC Teacher Fellowships to G.C. Goswami, M.R. Ghoshdastidar and S.K. Sengupta and UGC Research Fellowship to B. Ghosh through the University of North Bengal, India.

The financial assistance received from the Department of Atomic Energy, Govt. of India is thankfully acknowledged.

References

[1] D.H. Wilkinson, Proc. Cambridge Phil. Soc. 46 (1950) 508.

[2] F.F. Manfredi and A. Rimini, NAS-NRC Publ. 1184 (1964) p. 186.

Nuclear Instruments and Methods 199 (1982) 505–507
North-Holland Publishing Company

A SAMPLE–HOLD AND ANALOG MULTIPLEXER FOR MULTIDETECTOR SYSTEMS

G.C. GOSWAMI, M.R. GHOSHDOSTIDAR, B. GHOSH and N. CHAUDHURI
Department of Physics, North Bengal University, Darjeeling-734430, India

Received 1 June 1981 and in revised form 20 November 1981

A new sample–hold circuit with an analog multiplexer system is described. Designed for multichannel acquistion of data from an air shower array, the system is being used for accurate measurements of pulse heights from 16 channels by the use of a single ADC.

1. Introduction

There are various ways of realising sample-and-hold circuits and the analog multiplexer systems (e.g. refs. 1-5). In all cases detection of each peak for monitoring during sampling and holding the peak of selected pulses and then feeding it to an ADC through an analog multiplexer by controlling a logic state is not provided. In the present design, peak detection, holding and monitoring the channels are simultaneously made by means of a simple circuit. The circuit in its new form is always adjustable both for holding time of the peak during sampling and closing the input lines after a definite interval of time or instantaneously. Realisation of the analog multiplexer is made simply by FET switches operated by operational amplifiers and TTL ICs.

2. Principle of operation

Charging a storage capacitor up to a voltage equal to the peak of the analog pulse by means of a conventional peak detector, used in almost all cases of analog peak detection in analog systems, is utilised in the working principle of the sample-and-hold circuit. The voltage across the capacitor is retained for a few microseconds and then allowed to discharge through a switch for sampling. A "Hold" command cuts off the discharging path of the capacitor and the input line. This "Hold" command further connects the analog multiplexer consisting of FET switches and operated by logic pulses to the output of sample-and-hold units for scanning with an ADC.

3. Description of the circuit

The circuit diagram for the system is shown in fig. 1. The whole circuit is composed of two parts,

(1) sample and hold (S–H) unit comprising operational amplifiers (Op Amp IC-1 to IC-3), TTL ICs (IC-6 and IC-7), two field effect transistors (FET) T_1 and T_3, and a silicon transistor T_2 for each channel together with an Op Amp (IC-4) and TTC ICs (IC-8 and IC-9) for general control of all the input lines;

(2) analog multiplexer comprising TTL ICs (IC-10, IC-11) for channel address and decoding and an Op Amp (IC-5) together with a FET (T_4) and a diode to switch "ON" and "OFF" for each channel.

For each channel the analog pulse is fed to a peak detector unit consisting of an Op Amp (IC-1), a diode and a capacitor C and to the base of the transistor T_2 through a 10 kΩ resistor. The drain of T_1, acting as an input switch, is connected to the input line. Transistor T_2, acting as a logic level clipper, is to operate IC-6 with the input pulse. Transistor T_3 operated by IC-3 acts as a switch to discharge the capacitor C by triggering IC-7 after a definite time from the arrival of a pulse controlled by the pulse width of IC-6. The triggering of IC-7 is controlled by connecting the 'S–H command' to the reset input. The output of the S–H unit is taken by a voltage follower (IC-2).

The drain of the transistor T_4 acting as the first channel input of the analog multipexer unit is connected to the output of the S–H unit and to the gate of T_4 by a 120 kΩ resistor. The gate is connected to the output of a high slew rate Op Amp (IC-5) through a forward diode. A small voltage, about 1 V, is applied to the non-inverting input so that when the output of IC-10 is low the gate of T_4 goes to drain voltage and when the output is high the gate goes beyond the drain current cut-off value switching off the input output line. All the source terminals of the FET switches operating in the position T_4 for 16 channels are shorted to give the output. The sequential connection of the channnels is obtained by decoding the channel address with IC-10 generated by IC-11 which contains a channel advance instruction at the C_p input. R_D of IC-7, enable control (E) of IC-10. and R_0 of IC-11 are held high during

0167-5087/82/0000–0000/$02.75

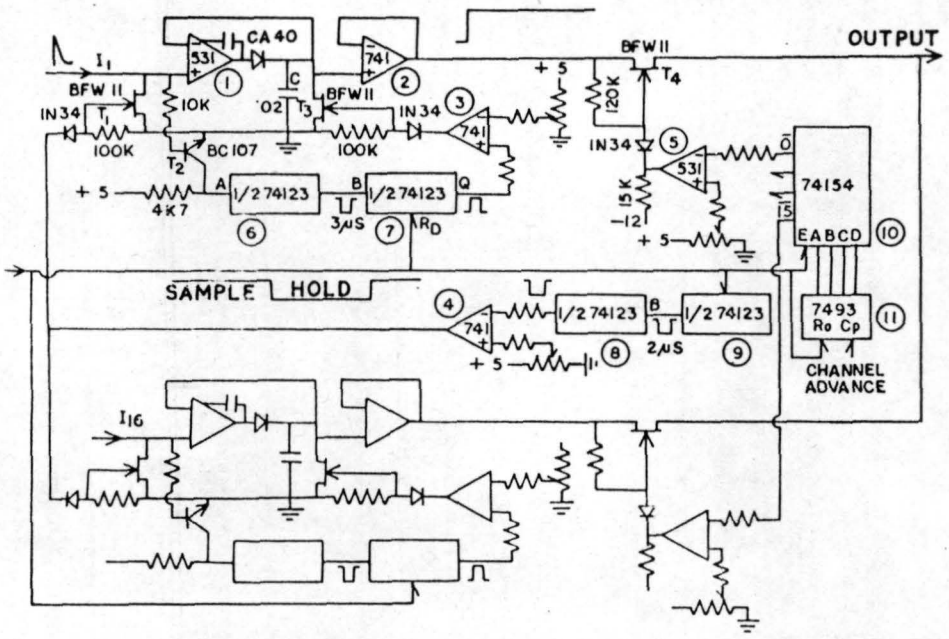

Fig. 1. Circuit diagram of sample-and-hold and analog multiplexer unit.

sampling and low on giving a "hold" command which closes the input line after 2 μs by operating IC-4 which makes the transistor T_1 conducting. The Q output of IC-6 of all the channels may be multiplexed and connected to a 7-segment LED display for monitoring (not shown in fig. 1).

4. Operation of the circuit

Analog pulses to be analysed coming from 16 detecting units are applied to the inputs I_1–I_{16}. Any analog pulse at input I_1 (say) will charge the capacitor C at a voltage equal to the peak of the analog pulse by means of high speed Op Amp IC-1 acting as a peak detector and is measured by the voltage follower IC-2. The drain current of transistor T_3 is normally cut off. The input pulse triggers IC-6 through transistor T_2 which produces a 3 μs width pulse. At the end of 3 μs, IC-7 is triggered to discharge the capacitor C by making transistor T_3 conducting. Thus the peak of each pulse is held for 3 μs during sampling.

As the "sample-and-hold input is held high during sampling 'enable controls' (E) of IC-10 and R_0 of IC-11 are also high so that IC-11 is at zero address and all the ouputs from the decoder (IC-10) are high. Thus all the outputs from S–H are cut off by the FET switch operating in the position T_4.

Normally, the control unit of the detector array where it is intended to be used contains TTL logic gates. The generation of a 'Hold Command' is almost instantaneous with the arrival of the selected pulses and hence falls within the sampling time of 3 μs. This 'Hold Command' makes R_D of IC-7, E of IC-10 and R_0 of IC-11 low; and at the same time it triggers IC-9 to produce a 2 μs width pulse. At the end of 2 μs, IC-8 is triggered to close all the input lines by making the input controlling transistor, in the position T_1, conducting. The width of the pulse from IC-8 must be greater than the time required for analysis. The input line is closed after 2 μs from the 'Hold Command' to ensure full peak value at the peak detector stage though it is operated by a fast operational amplifier. As R_D of IC-7 is low it will not trigger and the voltage across the capacitor C is retained. The wave form of the pulse after a "Hold" command is shown at the output of IC-2.

The "Hold" command connects the first channel to the output by making the output $\bar{O}$ of IC-10 low and counter (IC-11) ready for addressing the channels. All the 16 channels are analysed one after another by means of an ADC giving a channel advance instruction at the C_p input of IC-11.

During the whole cycle of operation, the input line is closed and therefore IC-6 will not be triggered which in turn keeps the "B" input of IC-7 high. The input "A" of IC-7 is permanently low. Hence, withdrawal of the hold command produces a low-to-high transition of R_D of IC-7. This transition of R_D when the "B" input is high and the "A" input is low triggers IC-7 to discharge the capacitor C.

5. Discussion

The "sample-and-hold" and analog multiplexer of the design described now is being operated in a cosmic

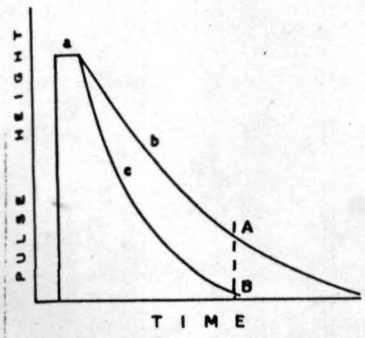

Fig. 2.Curve showing the discharge of the storage capacitor by a silicon transistor and a FET. (a) Width of the sampling pulse. (b) Discharge through the silicon transistor. (c) Discharge through the FET.

ray air shower experiment. The storage capacitor C should be large to avoid errors due to leakage when it is allowed to hold the voltage for a long time while an ADC scans all the voltages standing at 16 channels or even more when multiplexed. The optimum value of the capacitor is chosen at 0.02 μF to avoid "overshoot". During sampling the discharge of the capacitor C can be done by means of a silicon transitor by connecting its base directly to the Q output of IC-7 instead of using a FET. But with a silicon transistor the time of discharge of the condenser C is large compared to that for a FET as shown in fig. 2. The portion "a" in fig. 2 gives the width of the sampling pulse in an arbitrary scale and the two curves "b" and "c" give the discharge through a silicon transistor and FET respectively. At a particular time, indicated by the dotted line AB, if there is a "Hold" command when a high pulse is discharging af sampling, the "sample-and-hold" unit will hold the vo age present at that instant across the capacitor C resetting IC-7. Thus by using a silicon transistor t channel will give information of voltage equal to tl level A in the absence of any pulse in that chann Therefore in a fast detecting system a FET is alwa preferable to a silicon transistor. A high slew rate oper tional amplifier 531 is used to multiplex the voltages the output for making the voltage settling time mi mum. It is observed that the voltage settling time of t analog multiplexer is less than 10 μs.

The authors acknowledge the provision of facilit including UGC Teacher Fellowships to G.C. Goswa and M.R. Goshdostidar and a Research Fellowship B. Ghosh through the University of North Beng India.

The financial assist[illegible] received from the Dep ment of Atomic Energy, [illegible] India, is thankf acknowledged.

References

[1] A. Ogata, Nucl. Instr. and Meth. 115 (1974) 313.
[2] A.K. Chang and R.S. Larsen, IEEE Trans. Nucl. Sci. N (1973) 216.
[3] L.B. Robinson, F. Gin and H. Cingolani, Nucl. Instr Meth. 75 (1969) 121.
[4] M. Brossard and Z. Kulka, Nucl. Instr. and Meth (1976) 357.
[5] R. Bayer and S. Borsuk, Nucl. Instr. and Meth. 133 (185.

Random Access Memory with Programmer for Data Acquisition and Printing in a Multidetector System

B. N. Chaudhuri, G. C. Goswami, D. K. Basak and B. Ghosh

University Science Instrumentation Centre
University of North Bengal, Darjeeling 734430

The recording of data in Random Access Memory for the purpose of printing on a paper tape by a line printer in a multidetector system is described. The system is useful where printing of each set of data for a particular event is required to be accomplished. It is now being used in data acquisition from plastic scintillation detectors and magnetic spectrographs in cosmic ray air shower experiment, in the cosmic ray observatory at North Bengal University.

Today the RAM (Random Access Memory) is extensively used in storing programmed information in a computer or a microsystem. It is also used in storing data in multichannel and multiscaler analysers. In this present form, the digital information of the pulse height from a multidetector system of plastic scintillators is first stored and then printed by means of a line printer on a paper tape. The built-in-programme also has a provision for printing other digital information recorded in separate memories. These records are digitized muon triggered neon flash-tube glows for track recording as in the method of Ayre and Thomson (Ref. 1) and are printed in the octal system. The realisation of the built-in-programme is made by the use of monostable multivibrators, counters and set-reset latches. The circuit is very useful for recording of data from a number of detectors set for selected events such as in the cosmic ray air shower experiments.

Description of the Circuit

The circuit diagram for all the four systems is shown in Fig. 1. IC-1 to IC-4 are 4 1K (4x256) random access memories (MOS). IC-5 to IC-8 are decade counters to accept serial data output from an ADC with a programmer (Ref. 2). IC-9 and IC-10 are to address the memory channel. The outputs from the memory are not directly connected to the printer but through NAND gates serving the purpose of a multiplexer to accommodate data for printing from another unit (not shown in Fig. 1). The other unit in the present system is the memory that stores data from a magnetic spectrograph. Instead of NAND gates, two line to one line multiplexers may also be used. IC-11 to IC-23 together with set-reset latches and a number of gates constitute a programmer which controls the writing of the whole information in the memory and also gives the print command to the line printer to print all the information in the memory. The programmer also connects the magnetic spectrograph unit to the line printer. As shown in Fig. 1, the data from the magnetic spectrograph unit is received in an octal system. IC-11 delayed by IC-12 is used to reset the ADC output counters and to advance the memory channel by unity when the write command for each channel is withdrawn. IC-13, 14, 18, 19 act as preset counters to control the number of data items to be printed either from the magnetic spectrograph unit or from the memory unit. IC-15, 16, 20, 21 are retriggerable monostable multivibrators whose triggering is controlled by the set-reset latches R/S-2 and R/S-1 and give the 'print in red' and 'print in black' commands. IC-22, 23 initiate the 'print in black' command when the writing in the memory for all the channels is over and IC-17 initiates the 'print in red' command when the 'print in black' is over. All the inputs to the

THE AUTHORS

Dr. B. N. Chaudhari, Professor of Physics, Unversity of North Bengal (NBU), Darjeeling, has been responsible for the development of instrumentation for teaching and research in Nuclear Physics, Radiation Physics and Cosmic Rays, under a number of projects of the Department of Atomic Energy, Govt. of India and UGC. He has developed the University Science And Instrumentation Centre at NBU by acting as a part-time Head of the Centre since its inception in 1980.

Dr. G. C. Goswami was involved in the development of digital instrumentation at the centre under the Faculty Improvement Scheme UGC. A lecturer in Physics is one of the colleges under NBU, Dr. Goswami is now working on digital systems for the teaching laboratary.

Dr. D. K. Basak has been involved in the development of digital electronics for Cosmic Ray work at the NBU Centre.

Mr. B. Ghosh, Instrumentation Supervisor, has been working on instruments for teaching and research and has contributed to the development of digital systems at the Centre.

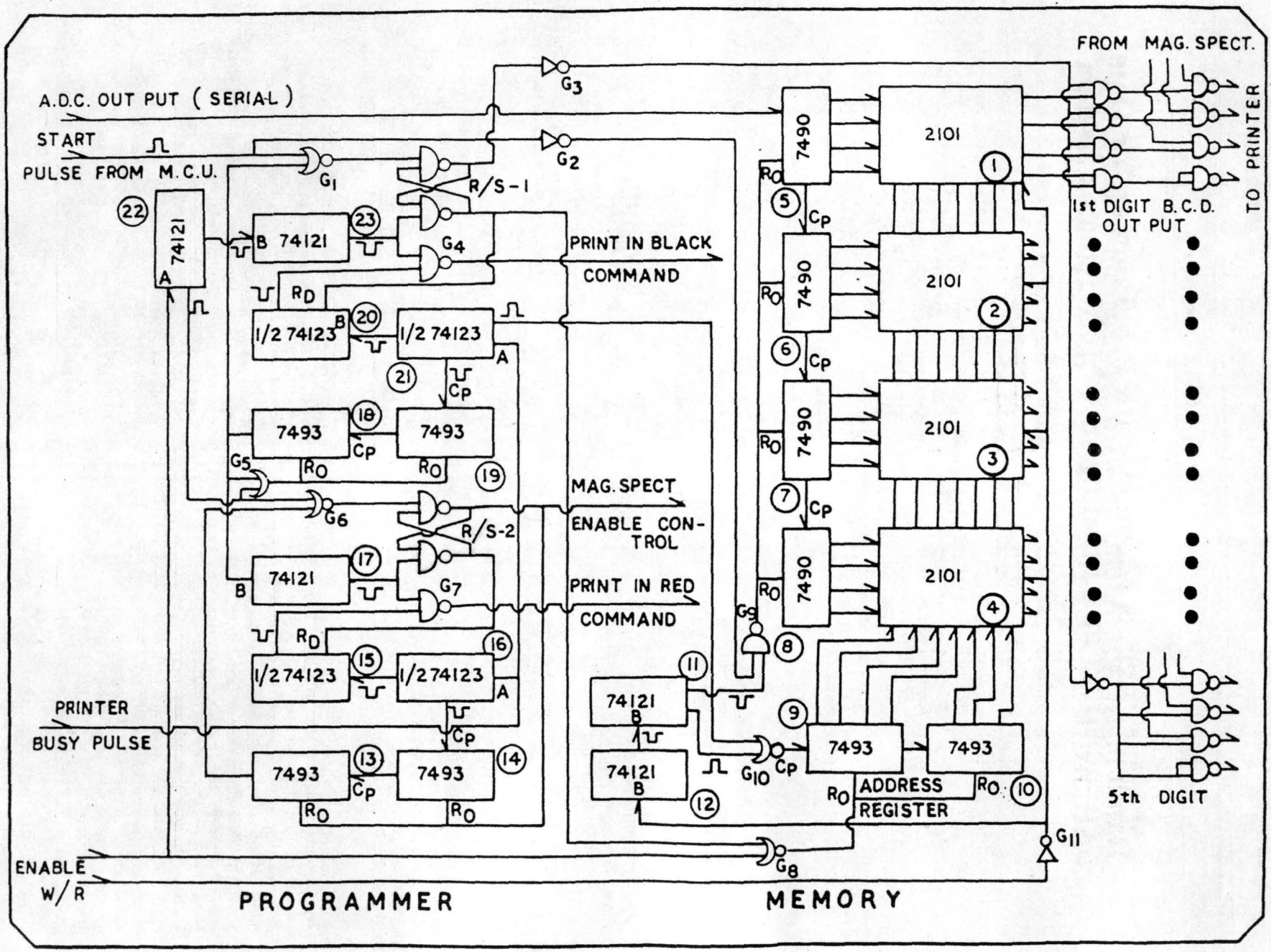

Fig. 1: Random Access Memory with programmer.

memory and the programmer are the outputs from an ADC with its programmer.

Operation of the Circuit

Whenever there is an event to record, the operation of the circuit is initiated by means of a start pulse from the master control unit (MCU) applied at the inputs of the gates G_1 and G_2. This start pulse resets all the counters, IC-5 to IC-8 to zero through G_9 and R_D of IC-20 and IC-21 low through R/S-1 to make them non-triggerable. The outputs of all memory ICs are gated off by R/S-1. The enable control is held high from the ADC programmer which allows connection of all the outputs from the detectors one after another to the ADC for scanning. As the enable control is high, the output of G_8 which controls the R_O of the memory address register is low for addressing the memory.

At the end of the start pulse, the ADC scan begins and the serial data output from the ADC enters the decade counters (IC-5 to IC-8). When the ADC scan for the first channel is over the programmer controlling the ADC gives a write pulse to the memory. This write pulse must be greater than 1 μs which is equal to the minimum write access time in case of a MOS memory. When the write pulse is withdrawn, it triggers IC-12 which in turn again triggers IC-11 to reset the decade counters and to increase the memory address by unity.

As the MOS memory does not operate with TTL speed so far as the mode for read and write is concerned, the resetting of the decade counters with the advancing of the address is delayed by about 1μs. This delay in the measurement of digital information of the pulse height will not affect the speed of operation since the analogue multiplexer (Ref. 3) which connects the ADC to the second detector output pulse always takes sometime known as the voltage setting time. The ADC scan for the second channel is now started and is stored in the corresponding memory address as in the case of the first channel.

When the ADC scan for all the channels is over, the enable control goes low and sets the memory at zero address through G_8 and triggers IC-22. The width of the pulse from IC-22 must be greater than 1μs to take care of the read access time of the memory. It also determines the time after which printing will start. The output from IC-22 resets the preset counters (IC-18 and IC-19) through G_5 and operates R/S-2 to make R_O of preset counters (IC-13 and IC-14) high and R_D of IC-15 and IC-16 low. IC-23 is triggered by IC-22 to give a 'print in black' command to the printer and to operate R/S-1 to connect the memory output to the printer through the multiplexer and to make R_D of IC-20 and IC-21 high. As soon as the printer gets the print command, the printer busy pulse goes high. At the end of the print, the printer busy pulse goes low and triggers IC-21 which advances the memory address and preset counter by unity and triggers IC-20 to give another 'print in black' command.

At the end of the required printing, the preset counter operates R/S-1 to stop the triggering of IC-20 and IC-21 by making R_D low and to switch off the memory output and connect the magnetic spectrograph unit to the printer. The preset counter also triggers IC-17 that gives a 'print in red' command to the printer through G_7 and operates R/S-2 to make R_D of IC-15 and IC-16 high. It also makes R_O of IC-13 and IC-14 and the enable control of magnetic spectrograph unit low.

As in the case of the 'print in black' command, 'print in red' commands are generated by IC-15 and IC-16 that are controlled by the preset counters (IC-13 and IC-14). After the end of the print of the whole information, the preset counters (IC-13, 14) operating R/S-2 stop further printing by making R_D of IC-15 and IC-16 low. The preset counter is also reset to zero and the whole system is ready for the next event.

Discussion

The Random Access Memory with the programmer of the design described here is being operated in the cosmic ray air shower experiment. The important feature of the circuit is that, one should be careful about the speed of operation of the MOS memory when it is operated by TTL ICs. Generally the read and the write access time of a MOS memory is greater than 1μs. Therefore, a print command to a printer, whose interface with TTL ICs to print the information from the memory should be delayed by a minimum time of 1 s after the change of address, so that the printer gets the information of valid data output from the memory. Therefore the pulse width of IC-21 and IC-16 must be greater than 1 μs.

In storing the data in the memory, the write pulse width should also be greater than 1 μs. The resetting of counters at the data input points and the change of address register of the memory should not be done simultaneously with the withdrawal of the write pulse but after a definite interval of time depending upon the memory characteristics. Therefore triggering of IC-11 is delayed by IC-12 after the withdrawal of the write pulse and this delay time may be some fraction of a microsecond.

References:

1. Ayre C A and Thompson M G, Nucl. Inst. and Meth., 69 (1969) 106.
2. Goswami G C, Ghosh B, Ghoshdastidar M R, Sengupta S K and Chaudhuri N, Nucl. Inst. and Meth., 192(1982) 375.
3. Goswami G C, Ghoshdastidar M R, Ghosh B and Chaudhuri N, Nucl. Inst. and Meth., 199(1982) 505.

North-Holland Publishing Company, P.O. Box 103, Amsterdam

Northprint:

Page 6 1st proof: 27 D

IN ALL CORRESPONDENCE CONCERNING THIS PAPER REFER TO:

NIM02642

6 JUN 1984

Nuclear Instruments and Methods in Physics Research 00 (1984) NIM02642
North-Holland, Amsterdam

A NEW MULTIDETECTOR SYSTEM WITH MAGNETIC SPECTROGRAPH FOR STUDY OF COSMIC RAY EXTENSIVE AIR SHOWER COMPONENTS

D.K. BASAK, N. CHAKRABARTY, B. GHOSH, G.C. GOSWAMI and N. CHAUDHURI

Department of Physics, University of North Bengal, Darjeeling, India

Received 29 November 1982 and in revised form 9 January 1984

An array of detectors for simultaneous observation of different components of cosmic ray extensive air showers (EAS) is described. The detector array, comprising plastic scintillation counters as electron detectors, magnetic spectrograph units and a muon flash tube chamber as muon detectors and a large volume multiplate cloud chamber as hadron detector has been set up and is now being operated at NBU campus. The array of detectors is sensitive to air showers initiated by cosmic primaries of energy in the range 10^{14} - 10^{15} eV.

1. Introduction

Nuclear multidetector systems continue to be of importance in ground based observatories engaged in high energy gamma ray astronomy and primary cosmic ray investigations. Very high energy primary gamma rays, protons or heavier nuclei have very low fluxes and consequently satellite studies are not feasible. The present status of observations using ground based techniques indicates a need for new and improved observatories at new sites. This paper describes a new ground based multidetector system that has been established for use in the search for high energy gamma rays and primary cosmic rays that develop into extensive showers of particles in the atmosphere.

2. Experimental arrangement

2.1. The air shower array

The relative position of each of the particle detectors is shown in fig. 1. The layout of the array is based on the arrangement of detectors in a square symmetry. The electron density detectors are scintillation counters constructed with BARC * plastic scintillators of two different sizes: 0.25 m^2 and 0.125 m^2. These detectors are arranged at various locations covering an area 600 m^2 in such a way that small-area detectors are near the centre of the array. The array set up on the ground level is located near a 10 m high magnetic spectrograph housing. This magnetic spectrograph housing limits the zenith angular acceptance of the incident showers to a few degrees.

The array set up also includes a cloud chamber (not shown in fig. 1) of size 1 m × 1 m × 0.8 m with 13 lead plates inside (thickness 1 cm each) as hadron detector and three GM counter trays (not shown in fig. 1) and one neon flash-tube chamber as muon detectors. A three-fold coincidence of any three adjacent detectors near the array centre produces a master pulse which triggers the data handling systems, high voltage flash tube units in the spectrographs and flash chamber muon detector and cloud chamber control unit.

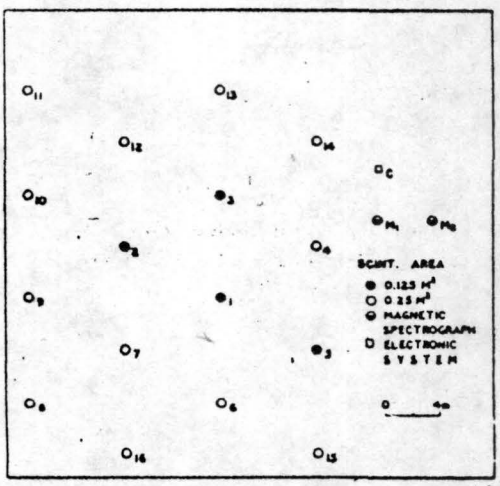

Fig. 1. Schematic diagram of air shower array.

* [illegible]oha Atomic Research Centre, Bombay, India.

REQUEST
Author, please indicate
- printer's errors in BLUE
- author's changes in RED

IMPORTANT
1. Please correct the proofs carefully; the responsibility for detecting errors rests with the author.
2. Restrict corrections to instances in which the proof is at variance with the manuscript
3. Recheck all reference data
4. A charge will be made for extensive alterations
5. Return proofs by airmail within **3 days** of receipt

Thank you.

2.2. Magnetic spectrograph units

Two magnetic spectrograph units at a separation of 4 m have been established in a housing which is located at a distance of 15 m from the array centre. Each unit is constructed using a rectangular solid iron magnetic block. These solid iron blocks were constructed [1] using low carbon content steel plates 12.5 mm thick. The plates are of size 180 cm × 125 cm with a rectangular hole of 19 cm × 35 cm at the centre. The thickness of the solid block thus formed by installing the iron plates one after another is 105 cm. The power requirement when wound with 600 turns of appropriate copper wire on the longer arms of the block and operated at 15 A current is 2.3 kW. Both longer arms of the magnet wound with wires have been used in the present investigation for deflection of EAS muons by using four accurately aligned muon flash-tube trays, two above an arm and two below, to locate the trajectory of the incident particle before and after passing through the solid iron magnet. The arrangement of the magnetic spectrograph is shown in fig. 2. An absorber of concrete and brick ~ 1 m thick on the roof about 1 m above the spectrograph units is provided to remove electronic components. Additional lead absorbers could be placed above the top tray of the spectrograph for this purpose. The information of the muon triggered neon flash-tube glows for the location of particle trajectories are obtained in digitised form. Each tray consists of eight layers of tubes which are staggered in such a way that a single particle passing through an array must traverse at least four trays (FT_1, FT_2, FT_3, FT_4). The tubes in each tray are placed in slots milled accurately in 'duraluminium' bars by means of a milling machine at CMRI **. The horizontal separation of the tube centres is 1.209 ± 0.002 cm which is referred to as one tube separation (t.s.). The vertical separation between the tube centres in a pair of adjacent layers is 2.8 cm. The flash tubes are 1.5 cm in diameter containing neon at a pressure of 60 cm Hg.A high voltage pulse of about 4.5 kV/cm with a rise time 0.75 μs is applied to the thin aluminium electrodes placed between layers of the tubes, 5 μs after the passage of a muon through the spectrograph by a trigger generated by the 3-fold coincidence of the scintillation counters (D_1, D_2, D_3). The tube discharges after the passage of the muon are recorded digitally and are printed on paper tape by means of a line printer. From the recorded coordinates of the passing muon at the four levels of detection in the spectrograph, its deflection in the magnetic field is calculated. The momentum of the muon is determined from the relation:

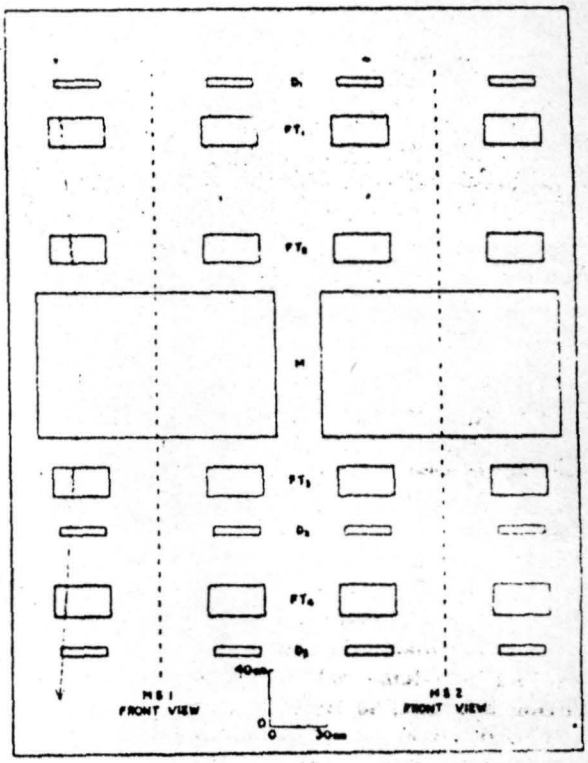

Fig. 2. Schematic diagram of magnetic spectrograph units.

$$P = 21.96/\Delta \text{ GeV}/c,$$

where Δ is the deflection in t.s. units and the constant in the numerator is the product of the geometrical factor of the spectrograph and the line integral of the magnetic induction. The maximum detectable momentum is given by

$$P_{\text{m.d.m.}} = \frac{21.96}{0.4266\epsilon_s} \text{ GeV}/c.$$

Its value is 440 GeV/c for $\sigma_s = 0.117$ t.s., the probable error in track location. The lowest momentum that can be measured with the spectrograph is 2 GeV/c.

2.3. Electron density detectors

The scintillators used in the detectors are of two different sizes: 0.5 m × 0.25 m and 0.5 m × 0.5 m with the same thickness of 5 cm. A Dumont 6364 photomultiplier tube mounted suitably to view the scintillator forms the detector. The pulses from all the 16 detectors are amplified by preamplifiers with a gain of ~ 20 each and are then sent to the main laboratory where they are again amplified by main amplifiers of appropriate gain. The main amplifier output saturates at 10 V, but the advantage of this amplifier is that it preserves the original shape after amplification except beyond the satura-

** CMRI: Central Mechanical Research Institute, Durgapur, India

tion region. In the next stage, this pulse is fed to the 'Sample and Hold' circuit [2] which keeps the pulse stored for about ~ 3 μs by charging a condensor. At the end of ~ 3 μs, this condenser discharges and is ready to accept information for the next event. Up to this stage all pulses from the detectors are accepted. The performance of each detector was studied while in calibration by measuring its single particle pulse height. The variation of pulse height from the centre of the detector to its edge was within ±10%. The differential pulse height spectrum for vertical muons has a standard deviation of 40%.

2.4. Flash-tube chamber: muon detector

This consists of 9 layers of neon flash tubes installed in a chamber with a cover of 5 cm lead to get rid of electrons. Each layer contains 54 tubes arranged in such a way that a single particle passing through the flash chamber must discharge the tubes lying on its trajectory. The flash tube chamber covers an area 1 m × 1 m for the location of the muon trajectories. The trigger pulse generated from the Master Control Unit (MCU) (fig. 3) is fed to the grid of a thyratron. The output pulse from the thyratron fires a second thyratron which in turn discharges a condenser (0.5 μF) charged to +12 kV through a 100 Ω noninductive resistor. The resulting high voltage pulse is applied to the electrode plates between the layers of the flash tubes. The master pulse from the 3-fold coincidence of the particle density detectors operates a relay for winding the film in the camera which records the glow information of the event photographically and also for paralysing the first thyratron for a certain interval of time. The internal efficiency of the neon flash tubes in the flash tube chamber is shown in fig. 4 as a function of delay time between the passage of the muon through the chamber and the air shower trigger pulse. An example of a flash

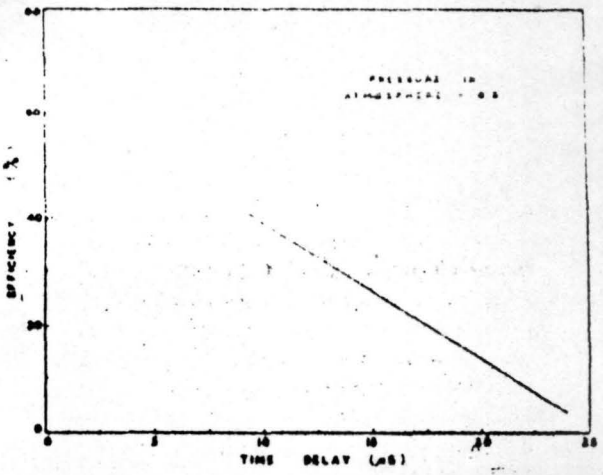

Fig. 4. Internal efficiency of the neon flash tubes as a function of delay time.

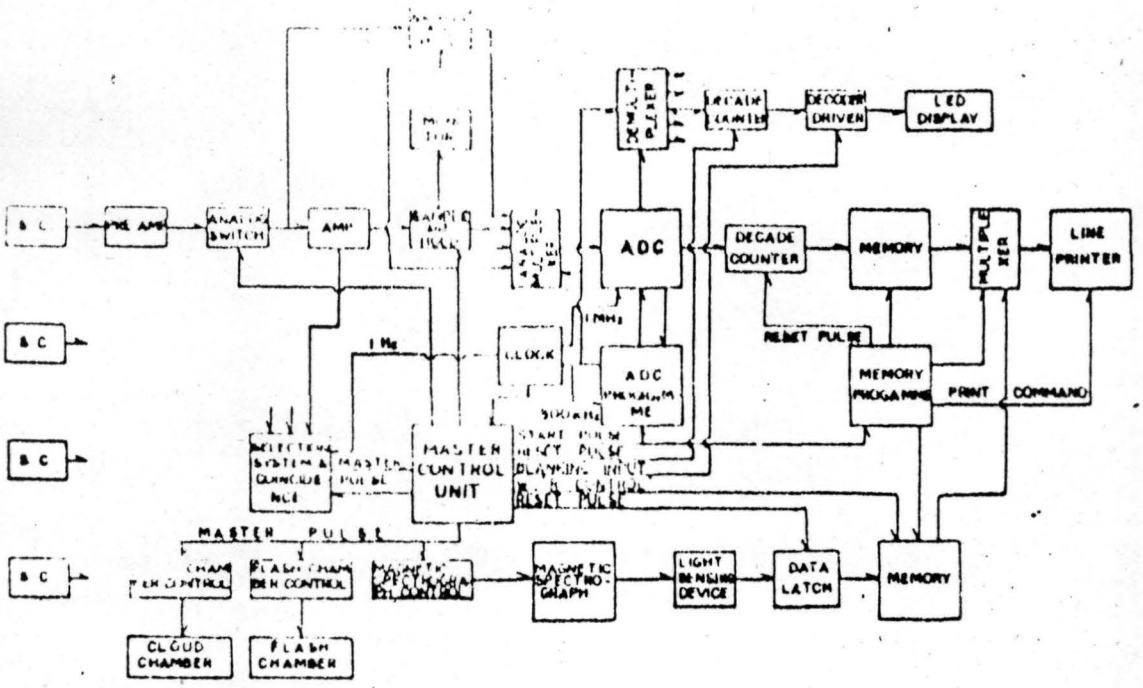

Fig. 3. Block diagram of electronic systems.

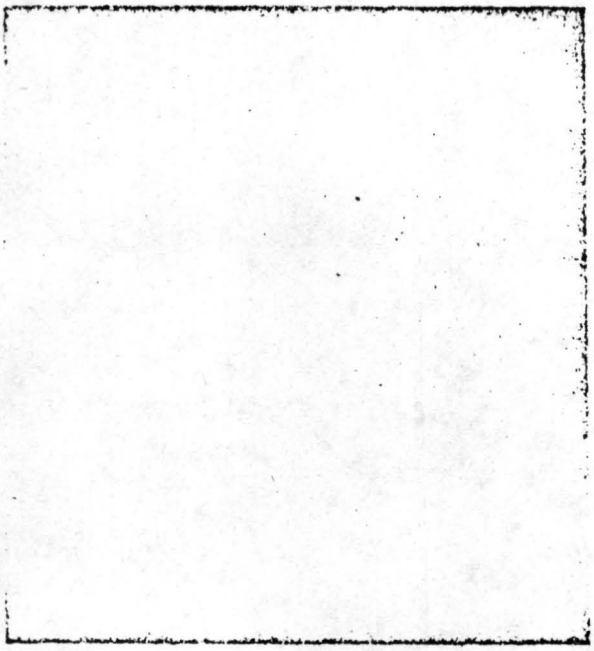

Fig. 5. An example of a muon track in the neon flash-tube chamber.

chamber record at the minimum delay time is shown in

3. Data acquisition, storage and transfer

Fig. 3 shows the diagram of the system for data handling in the NBU air shower experiment. The analog outputs from all the 16 detectors of the array after amplification first by preamplifiers and then by main amplifiers are fed to the 'Sample and Hold' circuits by charging capacitors for about ~ 3 μs after the triggering of the MCU by a master pulse generated from a 3 fold coincidence of any three of the adjacent particle density detectors in the array (detectors 1–7). At the end of 3 μs, these capacitors will discharge and will be ready to accept the next input pulses. When the MCU is triggered, it in turn triggers the multiplexer unit, the analog-to-digital converter (ADC), the ADC program unit and demultiplexer unit. They all will then be reset [illegible]. The multiplexer unit sequentially transfers analog [illegible] all the 16 Sample and Hold units to the [illegible] sequentially the analog pulses one after another. The time taken to scan all the channels is about 8 ms. The outputs from the ADC are demultiplexed by a demultiplexer whose outputs are connected to the display unit for visual display. The sequential outputs of the ADC are also connected to the memory unit for storing the digital information. After storage in the memory of all the information from the 16 detectors in the air shower array, these data are transferred to the printer for printing on paper tape. The adjustment is done in such a manner that a 10 V dc at the input of the ADC corresponds to a count of 1000.

The 3-fold coincidence master pulse also triggers the magnetic spectrograph control unit which then operates the spectrographs and the electrical information of the discharged neon flash tubes is fed, using suitable sensitive 'probes', to a separate memory unit. At the end of the printing of the air shower particle-density information from the 16 detectors, the digital information of each of discharged neon flash tubes is transferred from the memory to the printer for printing on paper tape.

We have also the provision for independent operation of the spectrograph. Here the spectrograph control unit is triggered by the 3-fold coincidence of the scintillation counter trays placed vertically [illegible] of the four arms of the spectrograph.

4. Operation and response of the array system

The master pulse generated from the coincidence of any three adjacent particle density sampling detectors triggers the MCU, cloud chamber control unit, magnetic spectrograph control unit and the flash-tube chamber control unit. As soon as the MCU is triggered it gives a 'Hold command' to the 'Sample and Hold' circuits, switches off the input lines by an analog switch and disconnects the coincidence circuit from the MCU and sends a start pulse to the ADC program unit.

Normally, the preset counters in the ADC program, the analog multiplexer, demultiplexer addresses are reset to zero and the ADC will not scan any input voltage, fed at its input. Once the ADC program unit is triggered, it connects all the pulses at the output of the 'Sample and Hold' circuits by an analog multiplexer one after another to the ADC. The analog pulse at the input of the converter will then charge a condenser of capacitance 0.1 μF by means of a constant current source (linear ramp generator) to a voltage equal to the input pulse amplitude to be measured. The charging time of the condenser to a voltage equal to the input voltage is measured by means of a 1 MHz clock pulse. When the ADC scan for the first channel is over, the memory program unit controlling the ADC gives a 'write' pulse to the memory for writing the digital information in the memory. As soon as the counting in the first channel is over, the ADC program initiates the multiplexer to connect the second channel to the ADC for scanning and then writing in the memory. In this way, it allows the connection of all the 16 channels one after another to the ADC for scanning and writing in the memory. For a visual check the digital outputs from the ADC for each channel are demultiplexed and dis-

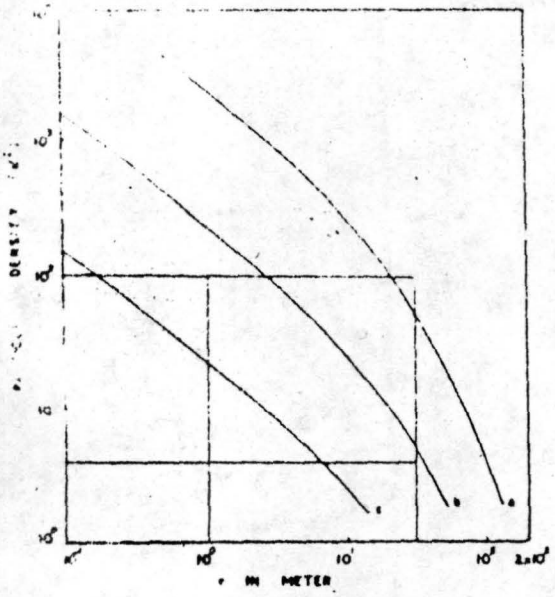

Fig. 6. Present response capability of the array. Shower size: curve (a) 10^5, curve (b) 10^4, curve (c) 10^3.

played by seven-segment LEDs. At the end of a 'write' pulse, a 'read' pulse is derived from the memory program unit which is then operating on the memory unit for recording the digital information on paper tape by a line printer.

One end of each neon flash tube is attached to a probe. The function of the probe is to convert the tube discharge information into electrical pulses. The electrical pulses carry the information about those neon flash tubes which are flashed due to passage of a muon through the flash tube trays. At the end of recording the information from the 16 density detectors and the discharged neon flash tubes, the analog switch is opened and it switches on the input lines for the next cycle.

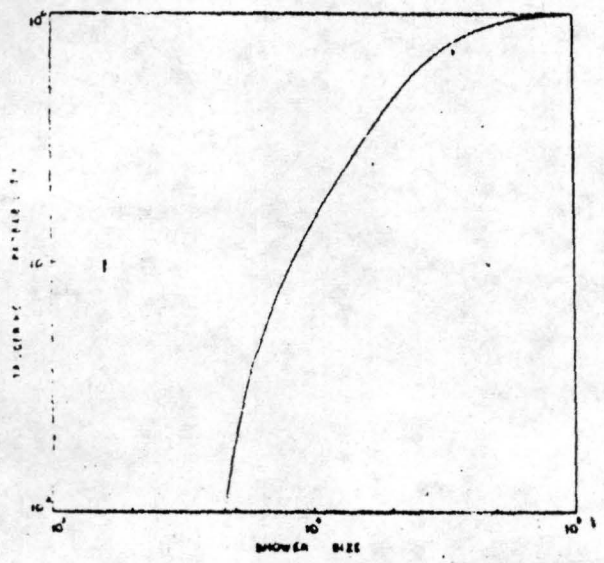

Fig. 7. The average triggering probability of the array of detectors as a function of shower size $s = 1.25$.

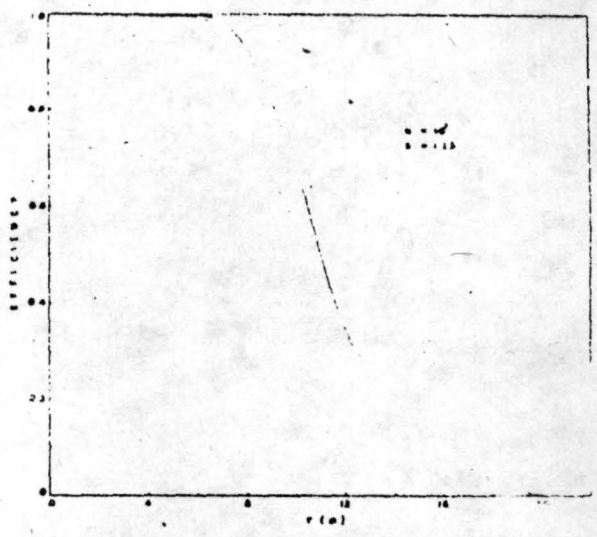

Fig. 8. The efficiency of detection of the array as a function of distance from the centre of the array.

The response capability of the array is shown in fig. 6 as the area bounded by four lines. Two horizontal lines show the dynamic range and the two vertical lines indicate the range of distance for density sampling. The present operation is being done by a trigger based on 3-fold coincidence under the threshold condition of one particle per detector. The average triggering probability for the array of detectors has been calculated as a function of shower size and s, using the Poissonian density distribution. The results for $s = 1.25$ and the triggering conditions on detectors within 8 m from the centre of the array shown in fig. 7. The efficiency of detection as a function of distance from the centre of the array is shown in fig. 8. This has been calculated on the basis of NKG function densities at the individual detectors, each superposed with a Gaussian error term. The fluctuating densities for each shower size and s are used to discover whether the shower satisfies the triggering conditions for its selection.

5. Conclusion

The array of detectors described is capable of recording simultaneously information about electrons, muons and hadrons in air showers arriving near sea level. The momentum spectrum of air shower muons in the range 2–440 GeV/c will be studied by two magnetic spectrograph units. The shape of the energy spectrum of muons

depends on the primary composition. If a correct model for high energy nuclear interaction is used for the calculation, a comparison of the measured muon spectra and the calculated spectra for different primary nuclei will enable a study of the mass composition of primary cosmic rays.

The Department of Atomic Energy, Government of India, is thanked for granting financial assistance for the construction of the apparatus and continuance of the work. The Department of Education, Government of West Bengal, has provided some financial assistance for this project.

References

[1] B.C. Nandi and M.S. Sinha, Acta Phys. Hung. 29, suppl. 4 (1970) 529.

[2] G.C. Goswami, B. Ghosh, M.R. Ghoshdastidar and N. Chaudhuri, Nucl. Instr. and Meth. 199 (1982) 505.

[3] G.C. Goswami, B. Ghosh, M.R. Ghoshdastidar, S.K. Sengupta and N. Chaudhuri, Nucl. Instr. and Meth. 192 (1982) 375.

17ème CONFERENCE INTERNATIONALE SUR LE RAYONNEMENT COSMIQUE
17th INTERNATIONAL COSMIC RAY CONFERENCE PARIS, FRANCE JULY 13-25 1981

CONFERENCE PAPERS

MN SESSION

VOL. 7

MN 4-11

NUCLEAR SHADOWING IN LEPTOPRODUCTION AND PHOTOPRODUCTION OF HADRONS

Ghosh B., Ghoshdastidar M.R.,
Basak D.K., Goswami G.C.
Chaudhuri N.

University of North Bengal
INDIA

ABSTRACT

New measurements of nuclear shadowing in leptoproduction and photoproduction of hadrons representing improvement in precision over earlier such experiments have been subjected to a critical analysis to examine their energy dependence and dependence on mass number. Several of the published calculations on nuclear shadowing have been considered by finding their predictions and by indicating the differences in their predictions and between predictions and measurements of shadowing in nuclear muoproduction, electroproduction and photoproduction of hadrons.

1. Introduction

Inelastic muon-nucleus (A) and electron-nucleus scattering measurements provide total photonuclear cross section ($\sigma_{\gamma A}$) for virtual photons. The photon shadowing 'S' in target nuclei expressed as ($\sigma_{\gamma A}/A\sigma_{\gamma N}$) (effective fraction of nucleons in the nuclear target) can thus be determined as a function of virtual photon energy E_γ and the square of four-momentum transfer q^2. The measurements of total cross-section for hadron production by inelastic lepton-scattering yield the effective fraction of nucleons in a nuclear target at very small q^2 -values but over a wide virtual photon energy range. These data together with the data from the real photoproduction experiments are taken together for testing existing calculations on nuclear shadow effect. Old experimental data on nulcear shadowing from real photoproduction experiments and also electroproduction experiments contain large uncertainties. New experimental data represent great improvement in the precision of measurements and appear to deserve a presentation which will exhibit a relation between various theoretical

predictions. In this paper, we attempt such a presentation considering the experimental data from recent measurements and latest theoretical predictions.

2. Nuclear shadow-effect calculations

The theory of shadowing of real and virtual photons in nuclei is based on

i) vector-meson dominant model in which photons are assumed to interact with nucleons via vector mesons.

ii) many-channel hadron-dominant model (generalised vector dominant model) in which photons are assumed to interact with nucleons via hadron states.

The pure 'Rho-dominant' calculation of photon shadowing has been given among others by Brodsky and Pumplin (1969). The multi-channel shadow-effects have been calculated neglecting off-diagonal elements between hadronic channels by Brodsky and Pumplin (1969). In the refined calculations of Cocho et al (1974), Distas et al (1975), Bezrukhov and Bugaev (1979), these off-diagonal terms have been shown to be significant in the case of heavier nuclear targets. The predictions of these calculations have not yet been mutually compared and tested adequately using reliable experimental data from shadowing of real and virtual photons in heavier nuclei.

3. Experimental data and analysis

We propose to examine photon shadowing through a study of (a) photon energy dependence on some target nuclei (A) and also (b) A-dependence for some photon energies using data from (i) cosmic-ray muon-nucleus inelastic scattering experiments (ii) accelerator electron-and muon-nucleus scattering experiments and (iii) real photoproduction experiments. The cosmic ray muon experiments provide total photonuclear cross-section at very low q^2 ($\simeq 0$) values over a wide virtual photon energy range. Experiments so far reported on inelastic electron-scattering and muon scattering have provided data at low q^2 values and have been combined with cosmic ray muon data for this analysis is based on

i) Measurements for virtual photons by

a) Lanik et al (1971)
b) Heynen et al (1971)
c) Bari et al (1975)

d) Eickmeyer et al (1976)
e) Baily et al (1979)

ii) Measurements for real photons by

a) Brooke et al (1973)
b) Daresbury report (1973)
c) UCSB report (1973)
d) Michalowski et al (1977)
e) Gabathuler E (1978)

To examine the data on the energy dependence and A-dependence, the data points with $q^2 \lesssim 0.1$ are plotted as a function of photon energy E_γ on some nuclei as shown in Fig. 1, and plotted as a function of A for several photon energies as shown in Fig. 2. The results are presented as fitted curves that represent the data well. The dependence of the data on A and E_γ is obtained in the form:

$$\sigma_{eff}/A) = 0.65 + 0.48A^{-.07} \cdot E_\gamma'^{-.49}, \quad E_\gamma' \text{ in unit}$$

of nucleon rest mass.

4. Comparison with theoretical predictions and conclusion

The theoretical predictions according to several of the calculations are displayed in fig. 3. Predictions of Brodsky and Pumplin (1969) above a photon energy of 5 GeV are higher than experimental data and those from the predictions of Distas et al (1975). The dependence of the shadowing on photon energy is seen to be very week. The shadowing observed in real photoproduction experiments is found to show a behaviour in qualitative agreement with that observed in low q^2 leptoproduction process.

References

1. Bezrukov and Bugaev 1979
2. Brodsky SJ and Pumplin J : 1969 Phy Rev. Vol. 182 No. 5 p 1794
3. Baily et al 1979 Nucl. Phy B 151 p 351
4. Brooker et al 1973 Phy Rev. D8 p2826
5. Cocho G et al 1974 Nucl. Phys. B78 p269
6. DESY report 1971 Physics Lett. 34B p651
7. Distas P et al 1975 Nucl. Phys. B99 p35
8. Eickmeyer J et al 1976 Phy Rev Lett Vol 36 No. 6 p289
9. Gabathuler E 1978 Proc. 19th Int. Conf. High Energy Physics;
10. Heynen V et al 1971 Phy Lett 34B p651
11. Lakin WL et al 1971 Phy Rev Lett Vol 26 p34
12. Michalowski S et al 1977 Phy Rev Lett Vol 39 No,12 p737
13. UCSB report 1973 Phy Rev D7 p1362
14. Paul A et al 1975 Proc. 14th Int. Conf. C. Hay, Munich, 1983

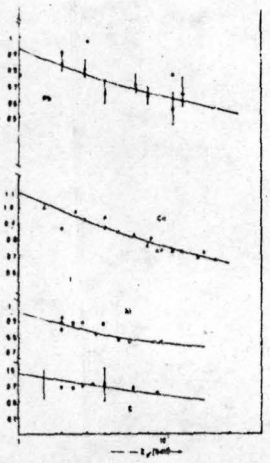

Fig. 1 (A_{eff}/A) vs E_r presented as fitted curves for various values of A. Data points from Refs. 3,4 & 8-13

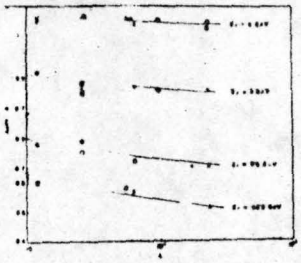

Fig. 2 (A_{eff}/A) vs A presented as fitted curves for various values of E_r. Data points from Refs. 3,4 & 8-13.

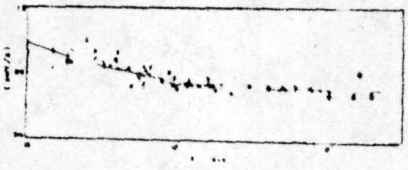

Fig. 3 (A_{eff}/A) for copper target compared with various theoretical predictions: — — Ref.(1); — · — Ref(5); - - - - Ref(1); —— Present work. Data points from Refs. 3,4 & 8-13.

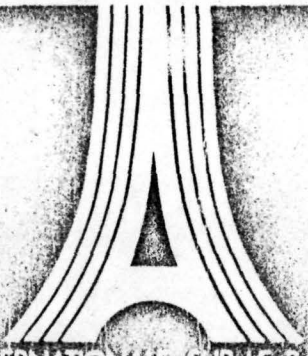

XVIIe CONFERENCE INTERNATIONALE SUR LE RAYONNEMENT COSMIQUE
17th INTERNATIONAL COSMIC RAY CONFERENCE PARIS FRANCE JULY 13-25 1981

CONFERENCE PAPERS

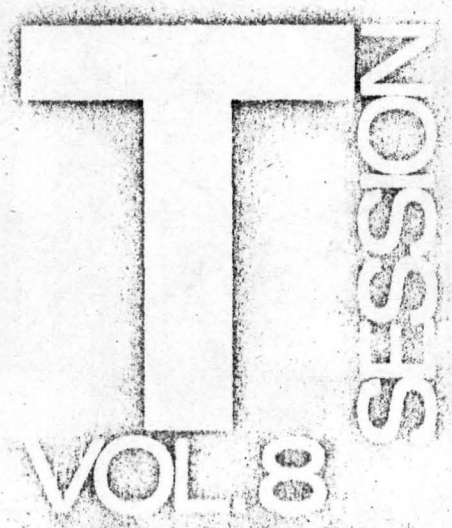

T 4-20

A PULSE HEIGHT RECORDING SYSTEM FOR SMALL AIR SHOWER ARRAYS

Goswami, G.C., Ghosh, B.
Ghoshdastidar, M.R.,
Basak, D.K.
Chaudhuri, N.
University of North Bengal
India

ABSTRACT

A pulse height recording system for a large number of channels from scintillation detectors of an air shower array has been designed, constructed and operated. In the present form of the system the digital output from individual channel is found to be linear upto 500 mV input. Each channel consists of a pre-amplifier, main linear-amplifier and a sample-and-hold. Each pulse height held by the sample-and-hold is scanned by the analog multiplexer and then digitised by an analog-to-digital converter. The digitised information is fed to a memory for printing on a paper tape.

1. Introduction

Analogue pulse from the array of detectors carrying particle density information is received by the pulse height analyser preconditioned by the selection system and operated by a master control unit. The block diagram as shown in figure 1 shows our present attempt to develop a system for recording pulse heights. The selected pulses are received, analysed and printed on a paper tape by means of a line printer.

2. Method

In the present form of the recording system, a pulse from each scintillation detector is amplified by a pre-amplifier consisting of operational amplifier of gain 20. The output pulse from pre-amplifier is further amplified by means of an amplifier of varying gain having an analogue switch at the input. Outputs from pre-amplifier and

amplifier are fed to sample and hold circuit, controlled by the master control unit. In the selection system, any three adjacent scintillators are taken to produce a coincidence master pulse to trigger the master control unit, cloud chamber control unit, Flash-tube-chamber control unit and Magnetic Spectrograph control unit. As soon as the master control unit is triggered it gives a hold command to the sample and hold circuit, switches off the input line, disconnects the coincidence circuit from the master control unit and sends a start-pulse to the programmed ADC and memory programme unit. The built-in-programme unit controlling the ADC, once triggered, connects all the pulses at the output of the sample and hold circuit by analog multiplexer one after another to the ADC for scanning. The digital outputs from ADC for each channel are de-multiplexed and displayed by seven-segment LED's for visual check and simultaneously recorded in a memory unit controlled by memory programme unit. The neon tube information of the magnetic spectrograph is received by a light sensing device which produces digital information. These output informations are stored in a memory unit.

The pre-amplifier and amplifier connected in our system are linear upto 10 V output. The output from the pre-amplifier is scanned to see whether there is any saturation at the output of the amplifier which will occur for large signal at the input. Since the pre-amplifier is of gain 20, the maximum voltage that can be recorded by scanning the pre-amplifier output by means of the ADC is 500 mV at the input point.

At the end of the ADC scan the memory programme unit produces a print command to the line printer and switches on the input line. The line printer first prints the digital pulse height and then the neon tube information of the magnetic spectrograph through a multiplexer controlled by the memory programme unit. At the end of the printing, the coincidence circuit is connected to the master control unit for the next event. The recording system of the cloud chamber and flash chamber are done by usual photographic method. Shower-frequency is recorded by connecting a scaler at the output of the coincidence circuit.

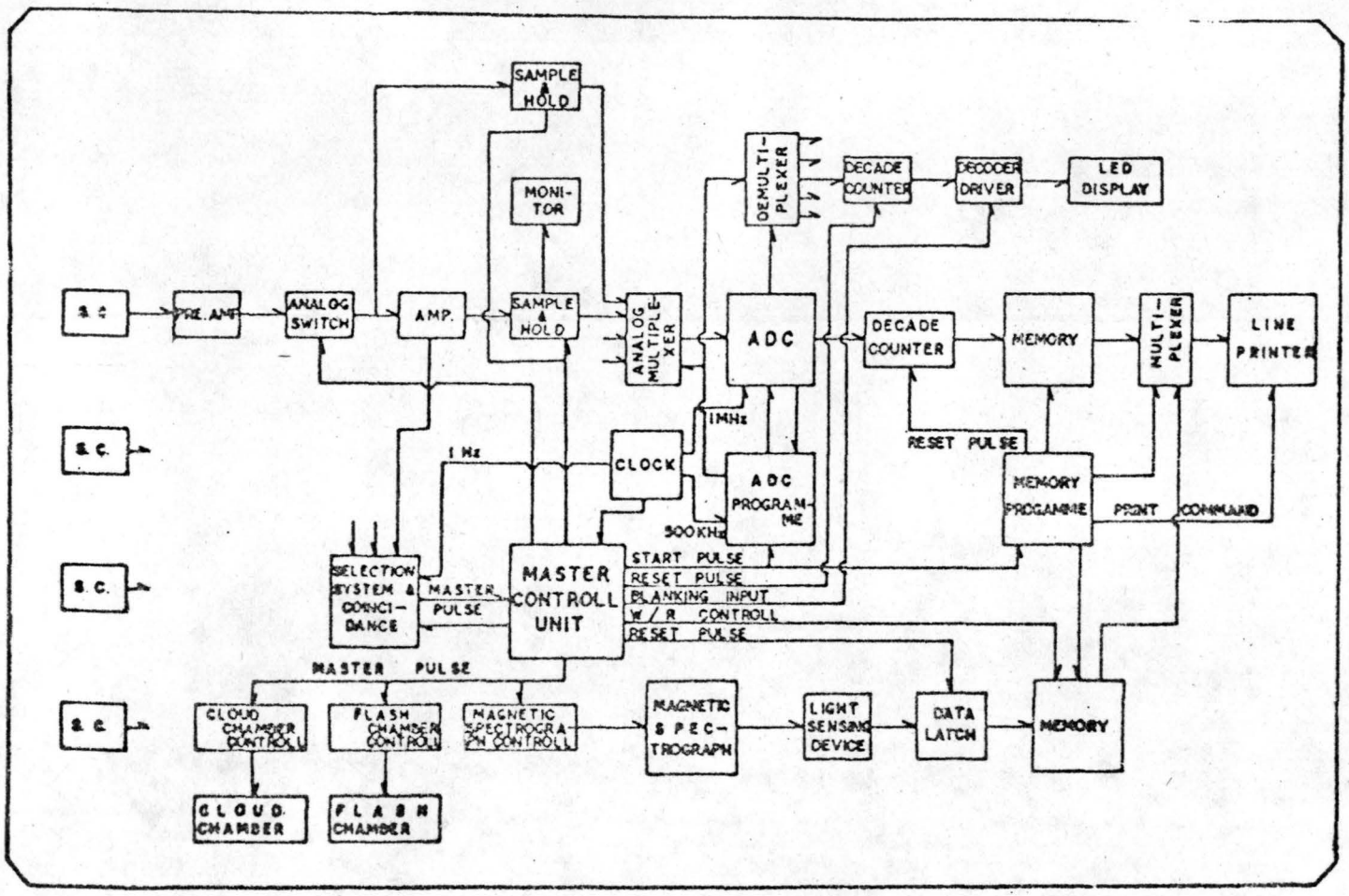

FIG. 1. BLOCK DIAGRAM OF ELECTRONICS OF AIR SHOWER ARRAY.

XVI INTERNATIONAL COSMIC RAY CONFERENCE

LOW ENERGY MUON SPECTRA NEAR SEA LEVEL

B. Ghosh, M.R. Ghoshdastidar and N. Chaudhuri
Department of Physics,
University of North Bengal, Darjeeling, India.

ABSTRACT

The inclusive cross sections for single meson production in proton-proton collisions have been used, together with the results of recent direct measurements of primary cosmic ray nuclei, to calculate the sea level muon spectra in the range 0.2-10 GeV. The calculated spectra are compared with the available vertical measurements near sea level to indicate the present status of the low energy muon data.

1. Introduction.

The vertical cosmic ray muon flux at sea level has been measured very precisely over a wide energy range 0.2 GeV - 1 TeV. Most of the low energy intensity measurements during 1970-1975 differ widely from those measured prior to 1970 (e.g. Gardiener et al, 1962; Allkofer et al 1971). Although there exist many measurements of spectrum in higher energy region, there are only two or three measurements of the spectrum in the energy region below 5 GeV. There are large discrepencies between the low energy measurements of Allkofer et al (1971) and of Gardener et al (1962).

The present paper gives low energy muon spectrum calculated by using the invariant cross-section data of single pion-kaon production in the inclusive proton-proton collision studied in the recent accelerator experiments. The calculated spectrum is compared with the measurements reported during 1970-1975 to explain the status of these measurements.

2. Method of calculation.

We have used the cross-section data for single charged pion and kaon production in the recent accelerator experiments on inclusive proton-proton collisions in the energy range 0.012-1.5 TeV to determine an expression for the invariant cross section in the form

$$E\frac{d\sigma}{dp^3} = A_1\left(1+\frac{1}{\epsilon_p}\right)^{-n} \exp\left(\frac{1}{\epsilon_p}\right).\ \exp\left(-B_1 x - C_1 p_t\right) \qquad \text{---- (1)}$$

where E_p in unit of $2m_p$ (rest mass of the p-p system) is the incident proton laboratory energy, p_t is the transverse momentum of secondary particle, $x = E/E_p$ (for $x \geq 0.02$) where E is the laboratory energy of the secondary particle. The values of the parameters of the fit to the whole set of the cross section data is given in our previous paper (Ghoshdastidar et al 1979). The

function (1) gives a good fit to the invariant cross section data for the whole incident proton energy range from 0.012 to 1.5 TeV. The p_t range is from 0.1 to 0.8 GeV/c over x=0.05 to 0.8.

We have used this cross section and incident nucleon spectrum based on recent direct measurements (e.g. E Juliusson 1975, for a compilation) to calculate the production spectrum of pions and kaons produced at the first primary nucleon-airnucleus collisions. Using such production spectra, the nucleon interaction mean free path $\lambda_I(80 g.cm^{-2})$ and attenuation mean free path $\lambda_a(120\ g.cm^{-2})$ in air, we solved (Ghoshdastidar et al 1979) the pion and kaon diffusion equations in vertical direction in the atmosphere to obtain the corresponding spectra as a function of atmospheric depth. The differential muon spectra at sea level due purely to decay of pions and kaons have been derived by introducing the probability that muons produced at the atmospheric depth X with energy E(X) can reach depth X_o with energy $E(X_o)$ along the vertical direction.

Our calculated results of the muon spectrum at sea level ($X=1030\ g.cm^{-2}$) for X values ($80\ g.cm^{-2}$, $230 g.cm^{-2}$, $280 g.cm^{-2}$) are shown in figure (1) for the purpose of comparison with the most recent measurements (Karmakar et al 1973, Allkofer et al 1973 Ng et al 1974, Flint et al 1973 Kong et al 1975).

Fig. 1.
Calculated low energy cosmic ray vertical muon spectra at sea level with the results of recent high precision measurements.

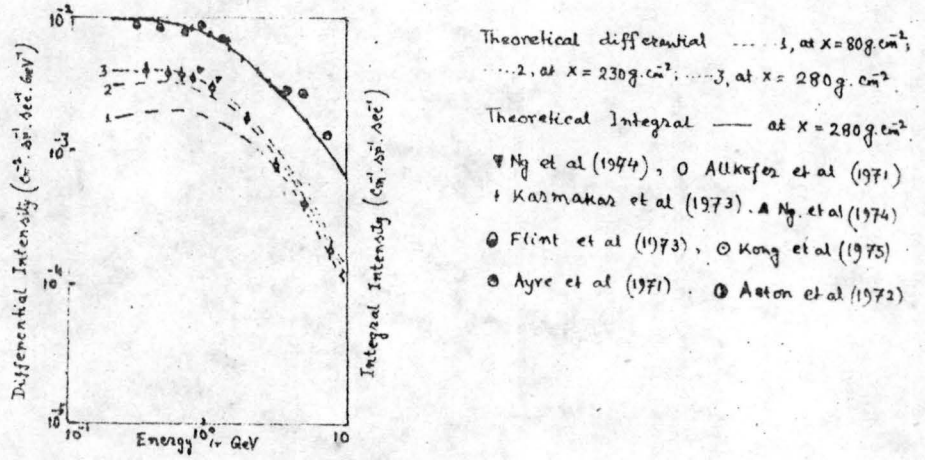

3. Comparison of data with measurements and discussion.

The measured differential and integral intensities from all recent measurements have been taken here for an evaluation in terms of the calculated sea level muon spectra. The latitude dependence of sea level muon flux has been taken into account in the measurements at locations where this factor is important. The effect of differences in time of measurements and meteorolo-

gical conditions could not be taken into account.

The figure (1) shows the shapes of the muon differential spectrum in the energy range below 10 GeV for three different values of muon production depth X. It is seen that most of the measurements are consistent with the calculated spectrum for mean depth X=280 g.cm^{-2} of air of muon production. The differential vertical intensities of muons at 0.375 GeV and 1.15 GeV by L K Ng. et al (1974) and intigral intensity at 4.75 GeV by Kong et al (1975) are found to be inconsistent with other measurements included in this analysis. The shape of the spectrum below 10 GeV is now determined and this work thus dispels the prevailing uncertainty (Gardener et al 1962, Allkofer et al 1970,1971; Thompson MG 1973, Aston et al 1972) regarding the low energy muon spectral shape.

4. Acknowledgements

The authors wish to thank the University of North Bengal for providing UGC research fellowship to B Ghosh and UGC Teacher Fellowship to M.R.Ghoshdastidar.

References

1. Allkofer C.C. et al 1971 Phy.Lett. Vol 36B N4 425 1973 Nuovocimento Vol.15 AN3 p353; 1970 Phy.Lett Vol.3B No.90 606.
2. Ayre C.A. et al 1971. J.Phy.A.L89.
3. Aston F et al 1972 Nuovocimento Vol 9B N2 p344.
4. Crookes J.R. et al 1972 Nucl.Phy. B 39 p493.
5. Flint R.W et al 1973 Phy.Rev. D8 N5 p1300
6. Gardener M et al 1962 Proc.Phy.Soc.Vol.80 pt.3 N 515 p 697.
7. Ghoshdastidar M.R. et al 1979 Nuovocimento (in press)
8. Juliusson E 1975 proc.14th ICRC, Munich EA Vol.8p1689.
9. Karmakar N.L. et al 1973 Nuovocimento Vol.17B N1 p173.
10. Kong D.P. et al 1975 Proc.14th ICRC, Munich Vol.8 MN 1.1(2)
11. Ng L.K. et al 1974 Nuovocimento Vol.22B N2 p328
12. Thompson M.G. 1973 Cosmic Rays at Ground level ed. A.W.Wolfendale.

5th